creative commons
COMMONS DEED

저작자표시-비영리-변경금지 2.0 대한민국

이용자는 아래의 조건을 따르는 경우에 한하여 자유롭게

- 이 저작물을 복제, 배포, 전송, 전시, 공연 및 방송할 수 있습니다.

다음과 같은 조건을 따라야 합니다:

저작자표시. 귀하는 원저작자를 표시하여야 합니다.

비영리. 귀하는 이 저작물을 영리 목적으로 이용할 수 없습니다.

변경금지. 귀하는 이 저작물을 개작, 변형 또는 가공할 수 없습니다.

- 귀하는, 이 저작물의 재이용이나 배포의 경우, 이 저작물에 적용된 이용허락조건을 명확하게 나타내어야 합니다.
- 저작권자로부터 별도의 허가를 받으면 이러한 조건들은 적용되지 않습니다.

저작권법에 따른 이용자의 권리는 위의 내용에 의하여 영향을 받지 않습니다.

이것은 이용허락규약(Legal Code)을 이해하기 쉽게 요약한 것입니다.

Disclaimer

dCollection

Ph.D. Dissertation of Engineering

The Study of Transient Responses of Nano Electrokinetics near Permselective Membrane

이온 선택성 막 주변에서 발생하는 나노전기동력학적 현상의 일시적 반응 연구

August 2020

Graduate School of Engineering
Seoul National University
Electrical Engineering and Computer Science Major

Soonhyun Kwon

The Study of Transient Responses of Nano Electrokinetics near Permselective Membrane

지도 교수 김 성 재

이 논문을 공학박사 학위논문으로 제출함
2020 년 8 월

서울대학교 공과대학원
전기·컴퓨터 공학부
권 순 현

권순현의 공학박사 학위논문을 인준함
2020 년 8 월

위 원 장 _____ (인)

부위원장 _____ (인)

위 원 _____ (인)

위 원 _____ (인)

위 원 _____ (인)

Abstract

The Study of Transient Responses of Nano Electrokinetics near Permselective Membrane

Soonhyun Kwon

DEPARTMENT OF ELECTRICAL ENGINEERING
AND COMPUTER SCIENCE
COLLEGE OF ENGINEERING
SEOUL NATIONAL UNIVERSITY

Nanoporous membrane has the perm-selectivity since the surface charge was affected the flow in the whole channels. The electrical potential derived from wall charge was formed in the entire channels and only counter-ions could penetrate, which is called perm-selectivity. Ion concentration polarization (ICP) is one of the perm-selective phenomena generated by difference of electrical potential in nanoporous membrane. Recently, the study of ICP was enormously increased from fundamental study to applications because of their utility in various fields. Especially, applications such as separator, desalination device and preconcentrator were largely researched and enhanced.

The applications were normally operated in transient state rather than

steady state. The characteristics of ICP in transient state have different from steady state and sometimes unexpected physical phenomena occurred. The phenomena could significantly disturb the performance of devices and reduce the efficiency. Therefore, the study of transient state was required. In this work, we studied the current characteristics of ICP in transient state to observe the ion transportation indirectly. And we continuously changed the boundary condition using pulsed electric field and investigated the ion transport using numerical simulation and experiments.

We investigated an overshoot current only found in transient state. The current-voltage curve of ICP has 3 regimes: Ohmic, limiting, and overlimiting current regime). The overshoot current unexpected high current is found between the Ohmic and limiting current regimes. We fabricated the noble device to observe the relevant of length of the effective microchannel and the overshoot current. And the current-voltage curve without the overshoot current was obtained in short time. We certified the relation between the diffusion relaxation time and the overshoot current by varying the microchannel length and the sweep rate of voltage.

And we observe the electroconvection in coercive transient state using pulsed electric field. The electroconvection is the significant physical phenomenon determining the current in overlimiting regime. The unstable vortices enhance the ion transport and current. For decades, pulsed electric field was applied to enhance the efficiency of ion transport with the advantage of reducing fouling effect of membrane, diminishing water splitting and

current enhancement. Among the advantages, the cause of current enhancement was still unclear and discussed. In this work we numerically simulated electroconvection and conducted experiments. Current density responses according to nondimensionalized frequency had the same tendency in both simulation and experiments. The current density was investigated based on ion transport derived from diffusion, drift, and convection. Furthermore, we considered the retardation effect since the boundary condition was consecutively changed. From this work, we could guess the convection retardation effect rather than restoration from diffusion was critical role in enhancement of current.

In this thesis, we conducted experiments and numerical simulation to investigate the fundamental study of ICP in transient state. We verified ion transport through the measurement of current and visualized the concentration distribution or the convection. Based on this thesis, the ICP applications could be more enhanced by simply changing the structure of device or applying optimal boundary conditions.

Keyword : Electrokinetics, ion concentration polarization, electroconvection, overshoot current, transient state.

Student Number : 2013-23098

Table of Contents

List of Figures

List of Tables

Chapter 1. Introduction

1.1 Permselective transportation in nanofluidics.

Permselectivity of nanochannels and nanoporous membrane was significantly related with the phenomena near the solid surface and electrolyte solution. When the solid surface is submerged in the aqueous solution, the surface bears the ions because chemical functional groups bonded on the surface are ionized or chemically adsorb the ions. Counter-ions in the aqueous solution approach to the surface to neutralize the charged surface of wall and co-ions are repelled from the wall. Consequently, a shallow layer composed of more counter-ions than co-ions is formed. The shallow ionic layer with the charges on the surface is called electrical double layer (EDL) [1].

From the Stern model, the electrolyte layer of EDL can be divided into two layers (**Figure 1. a**): Stern layer composed of immobile ions interfaced with surface of wall, and diffuse layer where the ions could freely move. Most part of EDL is diffuse layer and its thickness is determined by wall potential. Since the wall potential cannot be measured in experiment, the zeta potential (ψ_z), which is the potential at the shear plane near the solid-liquid interface, is used to study the electrical potential of EDL. From the Debye-Hückel approximation, electrical potential (ψ) near the wall is defined by

$$\psi = \psi_z \exp(-z / \lambda_D) \tag{1.1}$$

z is the distance from the wall and λ_D is the Debye length. The thickness of EDL is defined by λ_D where electrical potential is 1/e times the zeta potential. Debye length is

$$\lambda_D = \left(\frac{\varepsilon k_B T}{2e^2 z^2 n_\infty}\right)^{1/2} \tag{1.2}$$

where ε is dielectric permittivity of the solvent, k_B is Boltzmann constant, T is absolute temperature, e is elementary charge, z is the ionic valence, and n_∞ is bulk concentration[1]. From the equation (1.1), thickness of EDL is determined by concentration of bulk electrolyte and can vary from less than 1nm to a few hundred nanometers. When the electrolyte solution flows into a channel sufficiently larger than Debye length, EDL couldn't influence the whole channel. Therefore, electrical potential is zero in the channel except the vicinity of wall. Only a small number of counter-ions near the wall surface are affected by EDL, and most of the ions can pass through the channel without influence of EDL. However, electrical potential in whole channel is nonzero in case the electrolyte solution flows into a nanochannel or nanopore that walls are enough close to overlap the diffuse layers. Therefore, co-ions repel from the tunnels because of electrical repulsion and larger number of counter-ions than co-ions penetrate the tunnels, which act as a permselective membrane[2]. Electrical neutrality of ions in the nanochannel and nanopore is satisfied by wall charge in nanopore even if

the number of counter-ions is larger than the number of co-ions. As an example of the good ion selective membrane is Nafion which has narrow porous with high negatively charged wall [3, 4].

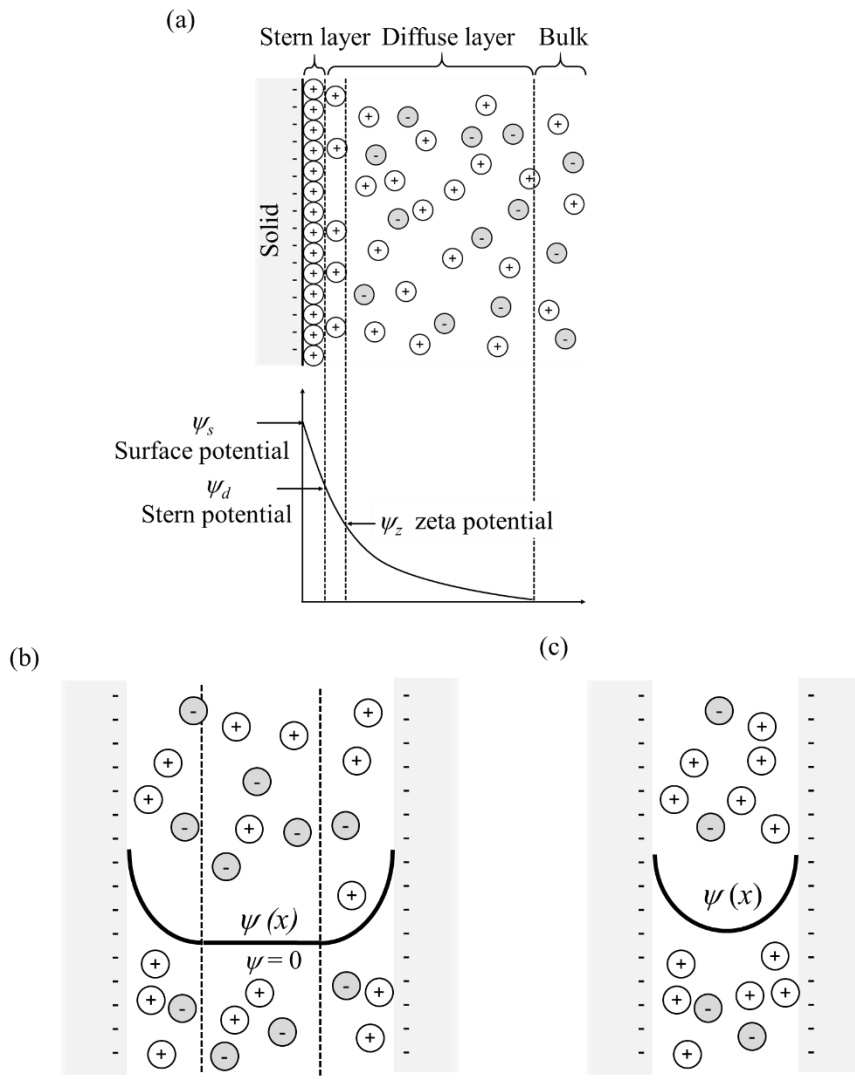

Figure 1.1 (a) Schematic of electric double layer and electric potential distribution. Electric potential and distribution of ions according to width of channel. (b) In the large, electric double layers cannot be overlapped, so ions could freely pass through the channel. (c) However, in the small channel, electric potential is nonzero, and few co-ions pass through the channel while the large number of counter-ions penetrate the channel.

1.2 Ion Concentration Polarization

Ion concentration polarization (ICP) is one of the permselective transport phenomena generated by the electric field[5]. Usually, ICP is utilized in the microfluidic application with the nanoporous membrane. When an electric field is applied to the permselective membrane connecting two individual microchannels, only counter-ions penetrate the membrane and concentration at both ends of the membrane changes. For instance, in the case of a cation selective membrane, only cation pass through the membrane. Remaining anion in the anodic side move apart from the membrane to satisfy the electrical neutrality. The net concentration of anodic side become almost zero and the depleted region is called ion depletion zone (IDZ). Meanwhile, cations that penetrated the membrane are accumulated on the other end of the membrane and anion also gather toward the edge due to electrical neutrality. Cathodic side has a higher concentration than bulk concentration and is called ion enrichment zone (IEZ). Forming of these two particular regions is called ICP.

The common experimental methods to study ICP phenomenon are measuring current with sweeping the voltage and observing the intensity of fluorescence dye added to trace the ion concentration. Since ions act as charge carriers in the aqueous solution, researchers can indirectly observe the change of concentration through measuring current. While the electric field is too strong that dyes cannot perfectly trace the ions in the vicinity of membrane,

researchers can indirectly obtain the concentration profile.

The representative property of ion concentration polarization is one of a kind current-voltage characteristics. Current - voltage curve can be divided 3 part; Ohmic regime, limiting regime, and overlimiting regime. First, current linearly increases as follow the Ohmic law. When voltage is applied on the membrane, anodic side of concentration decrease and become near zero. As the charge carriers are reduced, resistance of microchannel increases and current becomes constant though the voltage increases, which is called limiting current regime. And overlimiting regime is where the current increase again with higher voltage. The current increase is due to surface conduction, electroosmotic flow and electroconvection.

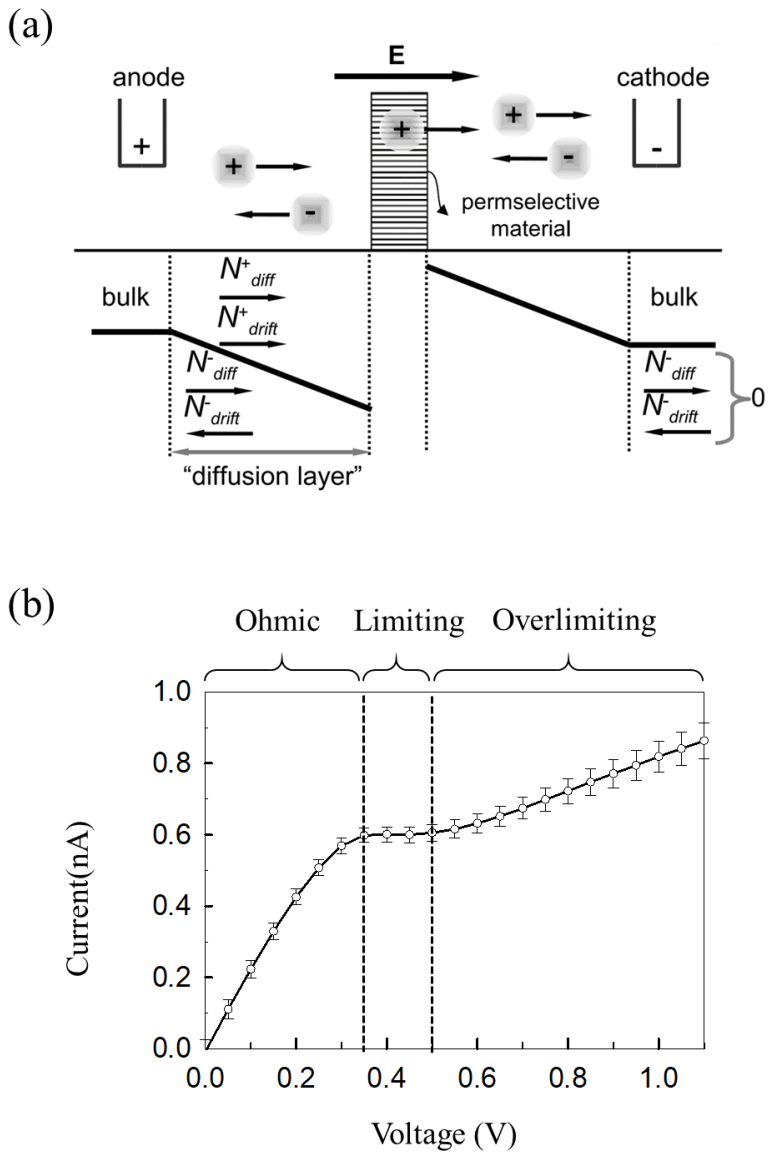

Figure 1.2 (a) Schematic of concentration distribution of ICP phenomenon [5]. (b) Experimentally obtained current-voltage curve of ICP devices.

1.3 Overlimiting current

In the limiting regime, ion depletion zone is formed and charge carriers are depleted. As the voltage increases, ion depletion zone is expanded, resistance becomes higher and the current keeps constant. However, current becomes increasing after threshold voltage which is called overlimiting current. There are 3 physical causes increasing currents: surface conduction, electroosmotic flow, and electroconvection (or electroosmotic instability)[6, 7]. Their effects are related with the characteristic length of microchannel.

In the narrow channel, the convection flow is negligible compared to diffusion. As high external voltage is applied, bulk concentration is reduced and bulk conductivity became low. However, counter-ions that screening surface charge are still kept that ions near the wall surface act as a main charge carriers, which is called surface conduction(SC) regime (**Figure 1.3 (a)**).

As the microchannel becomes thicker, the convection is influenced on the ion transport. Electroosmotic flow is generated in microchannel, the pressure-driven back flow is induced near the membrane and vortexes are generated like **Figure 1.3 (b)**. The vortexes are enhancing the ion transport and increase current. This is called electroosmotic flow(EOF) regime.

Lastly, if the thickness of microchannel is enough to thick to be less influenced by electroosmotic flow, the electroconvection is dominant in increase of current. Electroconvection is explained in detail in the next chapter. Electroconvection also occur the diverse vortexes that mix the concentration

and form current paths penetrating the ion depletion zone (**Figure 1.3 (c)**), which is called electroosmotic instability(EOI) regime.

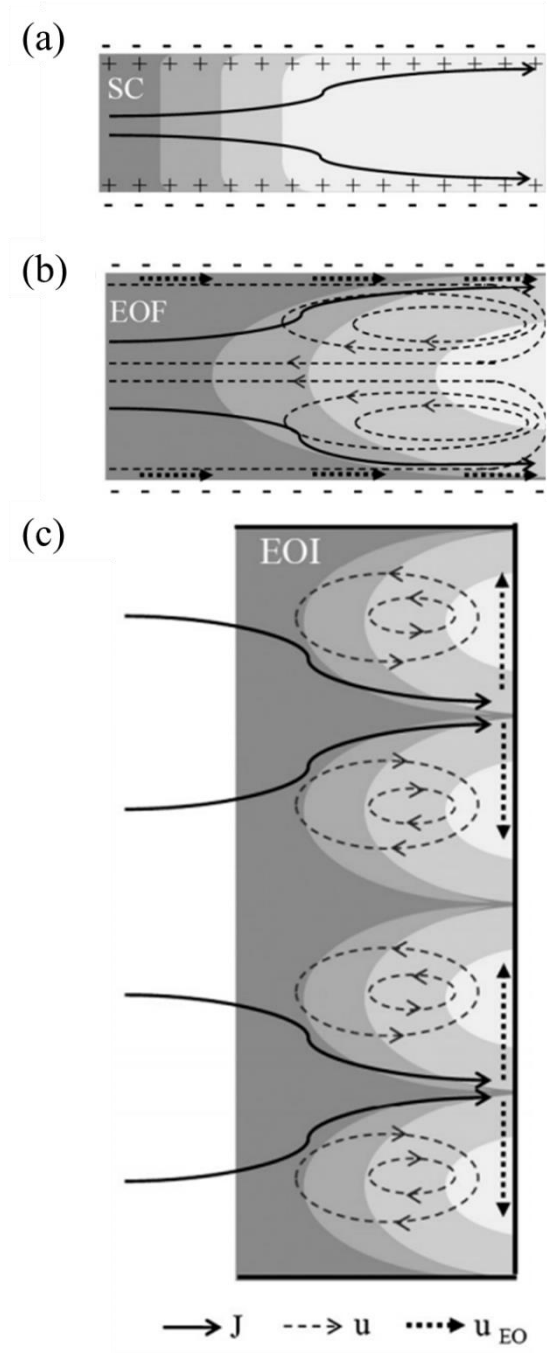

Figure 1.3 Schematic of ion transport and concentration distribution in microchannel in overlimiting regime. Electric field is applied from reservoir (left) to membrane (right) [6]. Current was determined by (a) Surface conduction, (b) electroosmotic flow, and (c) electroconvection.

1.4 Electroconvection

Electroconvection (electroconvective instability) is the unstable flow occurring in the IDZ under high electric fields. The electroconvection is generated by positive feedback of variation of concentration and differences of electrical potential[8] as **Figure 1.4 (a)**. Normally, when ICP occur with the plane membrane, there is the difference of electrical potential only in the normal direction of the membrane and there is no tangential flow near the membrane. However, with the high voltage enough to generate large depleted region, a non-electroneutral layer called extended space charge (ESC) layer is generated in the IDZ [9] and is formed in parallel with the membrane boundary (**Figure 1.4 (b)**). The charge of ESC layer is dependent on the wall charge of membrane. In the case of using a cation selective membrane, larger number of cation than anion exist in the ESC. Natural concentration perturbation exists in the ESC layer and this perturbation induce the small gap of electrical potential in the tangential direction of membrane (**Figure 1.4 (c)**). Then the ions of the ESC layer move along the electric field and the ESC layer becomes more polarized. Vortexes are also generated by the movement of ions in the ESC layer. These polarized ESC occur bigger tangential electric field and bigger vortex (**Figure 1.4 (c)**). These positive feedback is repeated and, finally, the huge concentration fluctuation occurs and fast vortexes are generated, which is called electroconvection.

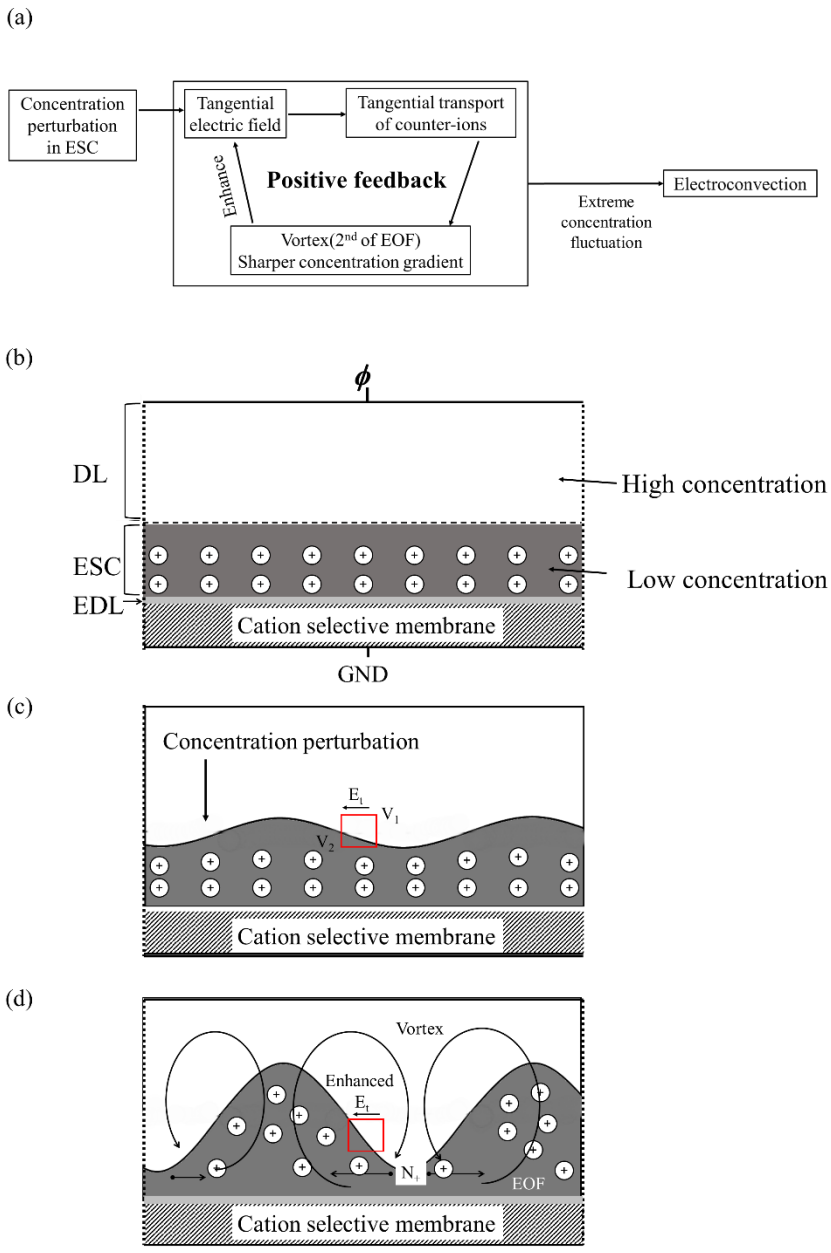

Figure 1.4 (a) The block diagram of the electroconvection and (b),(c),(d) schematic of the electroconvection. ESC has the large number of positive ions when ICP is generated using cation selective membranes.

1.5 Thesis objective

The various study of ion concentration polarization has been already conducted with the intensive attention. For decades, various fundamental study of ion concentration polarization was conducted [5, 6, 10-19]. Furthermore, researchers advanced the ICP applications with the high performance in various field such as biosensing[20], preconcentration[21, 22], particle separation[23, 24], water desalination[25-27], and fuel cells[28].

To enhance the ICP applications, researchers were studied the properties of both steady and transient state of ICP[6, 10, 11, 18, 28-30]. Especially, the study of ICP in transient state was very important considering that most ICP applications work in transient state rather than in steady state [21-24]. Nowadays, transient effect of ICP was studied such as propagation of ICP [31-33], preconcentration of charged species in ion enrichment zone[34], and pH change in ICP [35, 36]. However, Research into current response of ICP in transient state is still lacking. An overshoot current observed in transient state hides the optimal voltage of ICP application and disturbs the fundamental research of ICP in steady state [7, 37-39]. Also, the cause of current enhancement due to pulsed electric field is still discussed in numerous works [40-43].

In this work, we studied two transient properties of ICP. First, we investigate the overshoot current observed between Ohmic regime and limiting regime through experiments. The ICP applications were used the property of ion depletion zone where the charged particles were rejected. So,

the state of ion depletion zone determined performance of ICP devices. Therefore, the control of the ion depletion zone was significant. We usually know the state of ion depletion zone through measuring the current-voltage characteristic, but the measured current-voltage characteristic often has the overshoot current. We studied the critical factor of the overshoot current and suggested the noble devices in microfluidics. Second, the electroconvection with the continuously changing boundary condition was studied. Applying pulsed electric field has several advantages such as reducing the fouling effect and water dissociation, so researchers are already used in water desalination field. However, the physical cause of enhancement of current with pulsed electric field compared to with dc bias was still unclear. By studying electroconvection with the pulsed electric field, water desalination application can be enhanced their efficiency. Therefore, we numerically simulated and conducted the experiments about the electroconvection with pulsed electric field and suggest the cause of current enhancement.

.

1.6 Thesis outline

In this work, the study of ion concentration polarization was mainly describbed. In Chapter 1, we described the basic concepts of permselectivity and ICP. The significant property of ICP is described for Chapter 2. Furthermore, overlimiting current was described as details because we studied the different regimes of overlimiting current. Lastly, the electroconvection was described. Electroconvection is a kind of instability that is enormously studied for 20 years and studied in Chapter 3. Electroconvection is still unclear but we simply described how the electroconvection is generated theoretically.

In Chapter 2, we investigated the overshoot current in current-voltage curve of ICP. The overshoot current was theoretically related with the sweep rate of voltage, the length of diffusion layer and the diffusion relaxation time. In this work, we varied the length of effective microchannel where the concentration gradient is generated. The overshoot current was obtained over certain effective microchannel length at same sweep rate of voltage. We also varied the sweep rate of voltage to certify the relation between the diffusion relaxation time and the overshoot current. We could certify the relationship of the overshoot current with diffuse layer and suggest the noble devices for short time measurement.

In Chapter 3, electroconvection with pulsed electric field was observed. As the boundary condition was consecutively changed, the concentration and flow was affected by frequency of pulse. Both numerical simulation and

experiments were conducted and voltage was applied in overlimiting regime with electroconvection. We could obtain the optimal frequency of current density and we showed the maintenance of current path was the main cause of enhancement of current density.

Chapter 4 summarized and concluded the thesis.

Appendix A and B is relevant with Chapter2. Appendix A is about the convergence of current in overlimiting regime and compared the required time to steady state. Appendix B suggested that the overlimiting conductance according to length of microchannel.

Appendix C is the study of ICP application. We studied removal of diverse oil droplet using ICP separator. Appendix C showed the removal efficiency and suggested the critical value.

Chapter 2. The control of the overshoot current in ICP

2.1 Introduction

In recent years, permselective ion transportation through nanoporous membrane has been extensively studied due to its utility in various fields such as sensor [44] , separation [45], water desalination [26] and fuel cells [46]. One of major phenomena occurs near the nanoporous membrane is ion concentration polarization (ICP) which has received tremendous attentions by theoretical [9, 12, 47, 48] and experimental researchers [40-42, 49]. Because it provide the differential platform of the permselective migration near the membrane, one can deeply comprehend the behind mechanism of the movement using *in-situ* visualization of flow field / concentration distribution [30, 50] and direct numerical simulation [51, 52]. Based on these findings, one can precisely control the nanoelectrokinetic environment of such system for better engineering efficiency [14, 53-55].

ICP resulting from unbalanced ion transportation through the membrane can be directly characterized by the formation of an ion depletion zone and an ion enrichment zone at the anodic and cathodic side of the membrane in the case of cation-selective membrane [56, 57]. Furthermore, current-voltage (I-V) curve is most representing finger-print of ICP because of its distinctive transitions as a function of applied voltage. In a voltammetric measurement,

I-V curve has 3 distinguishable regimes (*i.e* Ohmic, limiting and overlimiting regime)[6, 7, 12, 27, 28]. Due to the lowest concentration inside the ion depletion zone, the ionic current was mainly determined by the properties of the ion depletion zone. In a micro/nanofluidic platform, however, an overshoot phenomenon (*i.e*. differential negative conductance) was easily observed at the transition from Ohmic regime to limiting regime as shown in **Figure 2.1(a)**[15, 37, 58]. ICP applications were operated at limiting regime or overlimiting regime depending on the situation. Since the current regime largely affected the ICP applications, the overshoot is a nuisance for the optimal performance in the electrochemical membrane system. Moya and Sistat have theoretically reported that the overshoot current in electrodialysis system can be eliminated by slowing the sweep rate of voltammetric measurement[59]. They also suggested that the required time to reach steady state was decided by diffuse layer length. However, in a micro/nanofluidic system, the length of microchannel was usually ~O(10) mm so that the required time to flatten overshoot current was over 10 hours at low concentration, which significantly impeded the nanoelectrokinetic study. Therefore, alternative approach was demanded for measuring proper I-V curve within a short time even with a microfluidic channel.

In this work, we fabricated the ICP device composed of two microchannels and nanoporous membrane as shown in **Figure 2.1 (b)**. The effective length (L_{eff}) of the main microchannel was coercively shortened by pumping fresh electrolyte solution through the side microchannels. As a result,

electrolyte concentration can be uniform along the main microchannel from left reservoir to the interconnected point with the side microchannels. By this manner, ICP layer can be formed only in the range from the interconnection to the nanojunction. Thus, we can achieve a coercive steady state for complete diffusion within the range of L_{eff}. By this mean, we demonstrated the diffusion relaxation time played a deterministic role for eliminating an overshoot phenomenon. Therefore, this simple but effective measurement platform would be a highly practical method to characterize the electrokinetic properties of permselective ion transportation because it can significantly save time and labor.

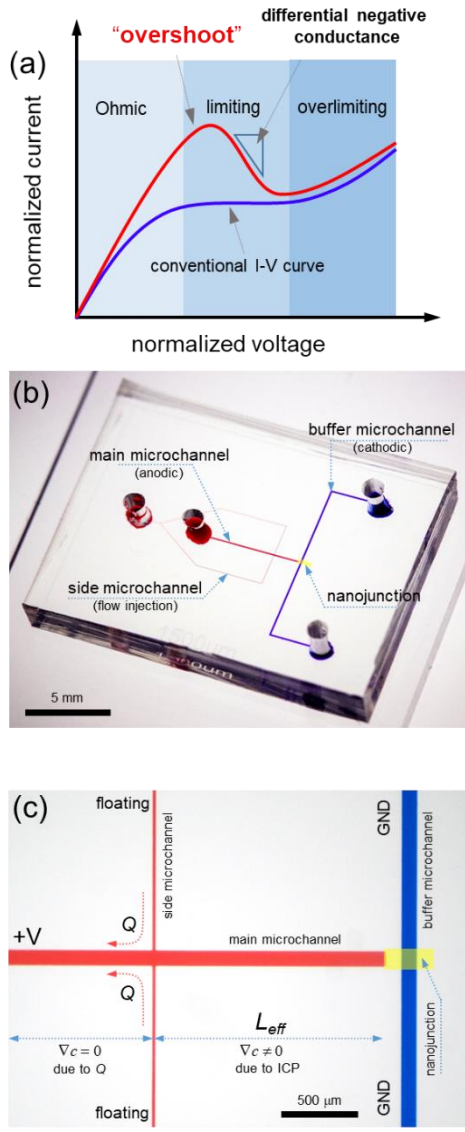

Figure 2.1 (a) Conventional (blue line) I-V curve vs "overshoot" phenomenon which possessed differential negative conductance. (b) Overview of micro/nanofluidic device. It had side microchannels to inject a fresh electrolyte to the vicinity of nanojunction. (c) Microscopic image of the device. Due to the fresh electrolyte injection, the electrolyte concentration should be uniform by L_{eff} away from the nanojunction.

2.2 Experimental Methods

Micro/nanofluidic devices were fabricated using soft-lithography with poly(dimethylsiloxane) (PDMS, Sylgard 184 silicon elastomer kit, Dow Corning, USA). Negative photoresist (SU8 2015, Microchem, USA) was coated on a 4 inch wafer to form a 15μm thick film for the device and 50 μm for the Nafion patterning microchannel. Soft bake was processed at 95 °C for 3 minutes to remove the organic solvent. Proper UV irradiation with predesigned mask was performed and the channels were developed using SU8 developer. Then mixture of PDMS base and curing agent (10:1 ratio) was poured on top of the wafers and was then solidified at 70 °C for 4 hr. Meanwhile, the blank microchannel (50 μm thickness, 100μm width and 1 cm length) was reversibly attached to a glass slide. Then, the microchannel was filled with Nafion solution (20 wt% resin solution, Sigma-Aldrich) by capillary force or negative pressure and the PDMS block was detached from the glass, referred to as a surface patterning method[57]. After curing the glass at 95 °C for 5 minutes, the solidified Nafion resin remained on the glass substrate. The fabricated PDMS microchannel and Nafion coated glass substrate were irreversibly bonded using a plasma bonder (CuteMP, Femto Science, Korea). Main- and buffer microchannel shown in **Figure 2.1 (c)** had the dimension of 100 μm width and 15 μm depth.

The most important feature in this work was the connection of the side microchannels. Electrically floated side microchannels were able to replenish

fresh electrolyte through a pump (PHD2000, Harvard). The dimensions of the side microchannel were 20 μm width and 15 μm depth. Therefore, the electrolyte concentration varied due to ICP in the range from the nanojunction to the injection point (*i.e.* L_{eff}), while the concentration was expected to be uniform out of the range as shown in **Figure 2.1 (c)**. We fabricated a number of device for different L_{eff} = 150, 300, 500, 650, 750, 1000, 1500 and 2000 μm.

For the initiation of ICP, external voltage (source measure unit, Keithley 236, USA) was applied through Ag/AgCl electrode connected to reservoirs (**Figure 1(c)**). I-V responses were measured by voltage sweep enabled by customized LabView program. The sweep rate of voltage was 0.05 V/30 sec from 0 V to 1.5 V for the main experiment and 0.05 V/1.5 sec ~ 0.05 V/60 sec for the sweep rate effect experiment. In the meantime, the propagation of ICP layer was visualized using an inverted fluorescent microscope (IX-51, Olympus, Japan) and a charge-coupled device (CCD) camera (DP73, Olympus, Japan). The obtained images were then postprocessed with CellSense (Olympus). For the fluorescent emission, 1mM KCl solution (Sigma-Aldrich, USA) with sulforhodamine B (SRB) (2 nM, Sigma-Aldrich, USA) was continuously injected from the side microchannels.

2.3 Results and Discussions

2.3.1 Electrokinetic response depending on L_{eff}

Main experiments were conducted with varying the position (L_{eff}) of interconnection where fresh electrolyte was continuously injected. Since the main microchannel was a dead-end configuration, infused solution flew only from the side microchannels to anodic reservoir as indicated in **Figure 2.2 (a)**. The flow rate was 3 μL/min. Therefore, the concentration profile of the main microchannel would have two distinctive parts. One from side channels to reservoir kept constant concentration (*i.e.* $\nabla c = 0$) due to the injected flow, and the other from the nanojunction to the side microchannels had a change of concentration (*i.e.* $\nabla c \neq 0$) as ICP was generated. The snapshots in **Figure 2.2 (a)** were captured after 6 minutes applying 1.5V, which was the highest voltage in this study in order to certify whether depletion zone would be suppressed between the nanojunction and the intersection. A black region represented the depletion zone of fluorescent dye. With L_{eff} under 750 μm, the depletion zone merely expanded which was considered pseudo-steady state, while it slowly expanded but was bounded by the side channels over L_{eff} = 1000 μm.

Under this circumstance, one needed to measure the electrical response of each configuration. **Figure 2.2 (b)** demonstrated the I-V characteristic from 0 V to 1.5 V with varying L_{eff}. When L_{eff} was 150 μm, I-V curve stayed in Ohmic regime until voltage reached to 1.5 V since hydroconvection

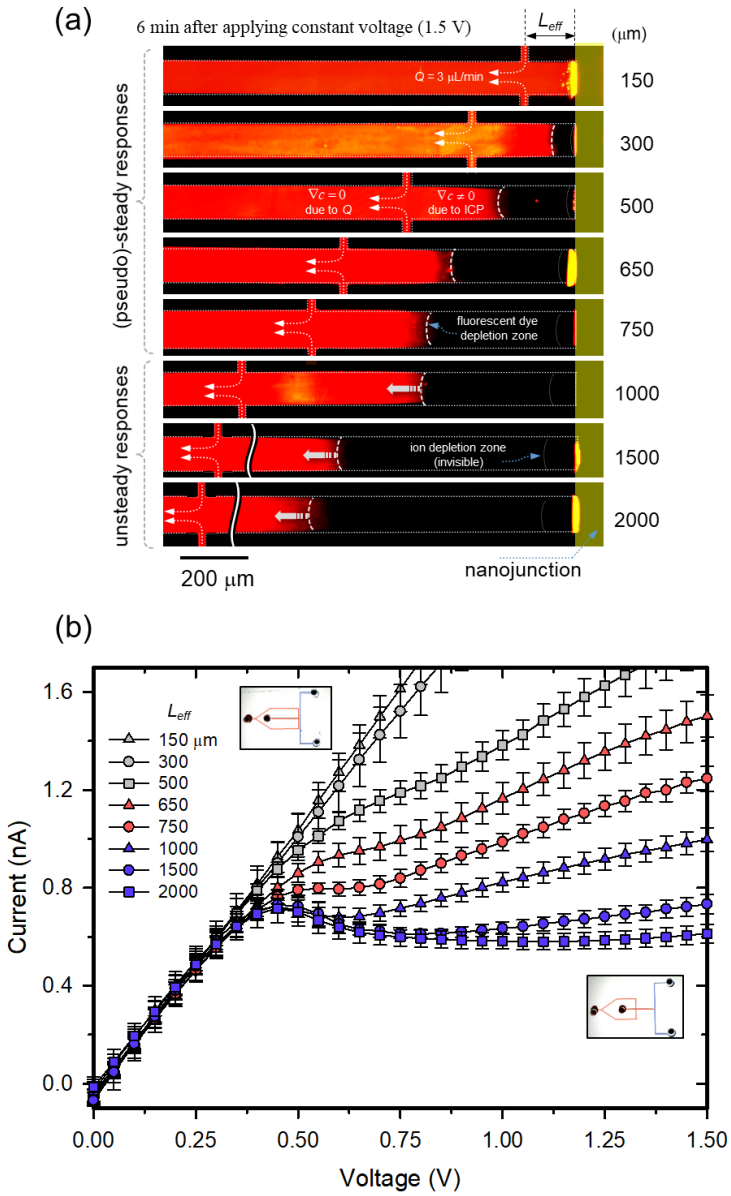

Figure 2.2 (a) Experimental visualization of ICP layer propagation as a function of L_{eff}. A constant voltage of 1.5 V was applied and the snapshot was captured after 6 minutes of applying the voltage. (b) Experimental measurement of I-V responses as a function of L_{eff}. The sweep rate was 0.05 V / 30 sec. The overshoot phenomenon was eliminated when L_{eff} = 650 and 750 μm. Over the range, I-V has significant overshoot.

circulated the concentration in diffuse layer as **Figure 2.3 (a),(b).** When L_{eff} was 300 μm and 500 μm, I-V curve was changed from Ohmic regime to overlimiting regime without limiting regime. Since hydraulic convection caused by injected flow from the side microchannel completely (or largely) suppressed the propagation of ICP layer, I-V response had a long Ohmic regime and a direct jump to overlimiting regime without limiting current response [15]. Interestingly, I-V curve had three distinctive regimes without overshoot current when L_{eff} was 650 and 750 μm. The effect of hydroconvection derived from side channel was restricted and didn't directly affect the effective microchannel. Under the steady state assumption, we can compare the experimental limiting current value with an analytical expression[5] of $i_{lim} = 2FDc_0A/\delta$ where F the Faraday constant, A the cross-sectional area of microchannel and c_0 the bulk concentration as shown in **Table 2.1**. The difference between $i_{lim,theo}$ and $i_{lim,exp}$ was under 7 % in the case of L_{eff} was 650 and 750 μm. When L_{eff} exceeded over 1000 μm, overshoot was generated and $i_{lim,exp}$ was much higher than $i_{lim,theo}$ leading to erroneous electrokinetic responses when there is the overshoot phenomenon.

L_{eff}	$i_{lim,theo}$ (nA)	$i_{lim,exp}$ (nA)
650	0.89	0.90 - 0.95
750	0.77	0.76 - 0.80
1000	0.58	0.68 - 0.72
1500	0.39	0.61 - 0.73
2000	0.29	0.58 - 0.72

Table 2.1 Theoretically calculated and experimentally measured limiting current value depending on L_{eff}.

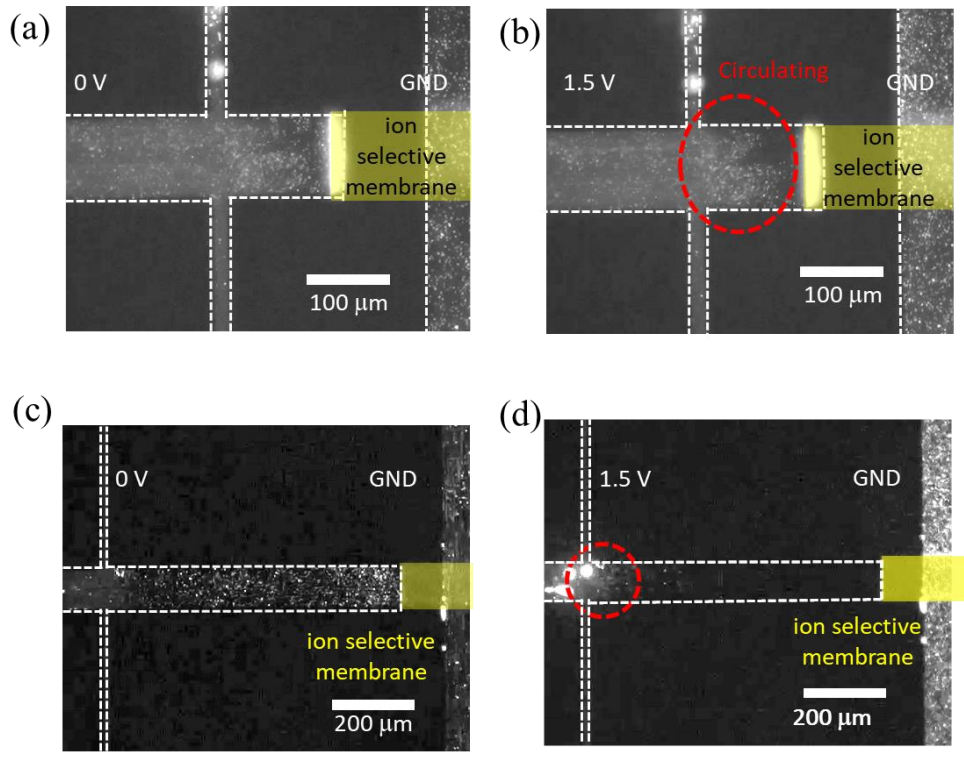

Figure 2.3 (a),(b) The picture of the hydroconvection at L_{eff} = 150 μm and **(c),(d)** L_{eff} = 750 μm with applying voltage 0 and 1.5 V respectively. The hydroconvection affected the whole channel and the diffuse layer couldn't fully expand in the effective microchannel when L_{eff} is under 500 μm. The hydroconvection only affected the entrance of effictive channel when L_{eff} is over 650 μm

2.3.2 Diffusion relaxation time in a microchannel of L_{eff}

Diffusion relaxation time of ions in the occurrence of overshoot current in voltammetry was reported to have a close relation with the response of ion flux in the main channel[59]. In Ohmic and limiting regimes, all of convection was negligible and most of electromigration affected the small portion of microchannel (*i.e*. the ion depletion zone which is invisible in **Figure 2.2(a)**). Therefore, we only considered the relaxation time of diffusion for characterizing the overshoot effect. The analytical expression for the diffusion relaxation time, τ_D is δ^2/D where δ is the length of diffuse layer in steady state and D is the diffusion coefficient of ion. As L_{eff} increased, the diffuse layer at steady state and the diffusion relaxation time would also be longer.

To verify this scenario, we conducted I-V measurement as a function of various sweep rate of voltage as shown in **Figure 2.4**. I-V curves with fast sweep rate had a higher current value and an overshoot phenomenon on a whole. This relationship can be explained by classical cyclic voltammetry theory[60]. The peak current at the overshoot scales as square root of voltage sweep rate[59]. Note that the scaling (RT/zFs : s is sweeping rate) in classical cyclic voltammetry theory is off by a factor of 20 or so to our diffusion time. The factor of 20 actually comes from the fact that the characteristic voltage for the diffusion time is not (RT/zF)~24 mV but rather the voltage of the experiment for depletion by a membrane. RT/zF is a typical voltage drop for electrochemical reactions in cyclic voltammetry but not so for membrane

depletion. In fact, if one uses the voltage at limiting current listed in the response, 0.4 to 0.7 V, these voltages are about 20 times RT/zF. Thus, the overshoot is due to the advancement of the depletion front, which is quite analogous to the advancement of a diffusion front in cyclic voltammetry. The only difference is the characteristic voltage used. This would be a nice connection between an ion-selective membrane and an ion-selective electrode. In this work, however, as the sweep rate slowed, peak currents tended to decrease and overshoot was diminished. The maximum sweep rates to eliminate the overshoot were 0.05 V / 10 sec, 0.05 V / 30 sec and 0.05 V / 60 sec for L_{eff} = 500, 750 and 1000 μm, respectively. Without occurrence of overshoot, the voltages required for initiating limiting current were 0.7, 0.5 and 0.4 V, respectively. Thus, it took 140, 300 and 480 seconds to reach these voltage values in the experiments. These values were well matched with theoretically estimated τ_D which was summarized in **Figure 2.4**. Therefore one need to set the sweep rate as the ions can diffusively transport only within the effective length of microchannel, not the entire length of microchannel, which dramatically reduce the I-V measurement time and labor.

L_{eff}	500 μm	750 μm	1000 μm

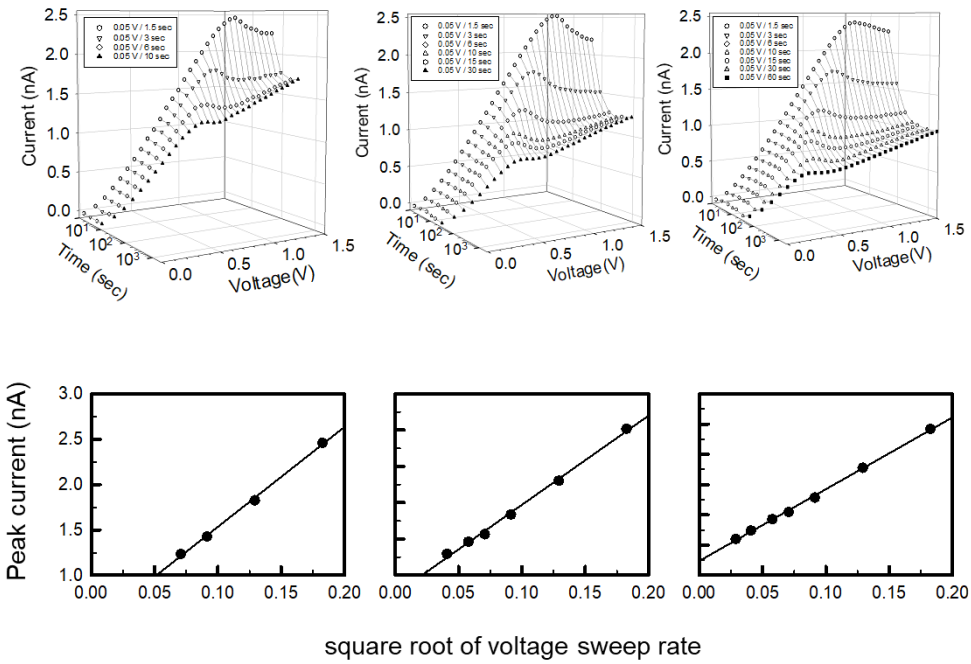

maximum sweep rate for no overshoot[a]	0.05 V/10 sec	0.05 V/30 sec	0.05 V/60 sec
voltage required for i_{lim}(V)[b]	0.7	0.5	0.4
$\tau_{D,exp}$ (sec)[b/a]	140	300	480
$\tau_{D,theo}$ (sec)	125	280	500

Figure 2.4 Table of I-t-V responses for varying L_{eff} and the sweep rate. From the plots, one can estimate the minimum sweep rate for disappearance of overshoot. The rate has a close relationship with the diffusion time of ions in a microchannel.

2.4 Conclusion

In this work, we developed a new measurement platform for I-V characteristics of permselective ion transportation. It has been reported that an overshoot phenomenon impeded the correct electrokinetic responses in micro/nanofluidic device, because it represented a differential negative conductance. In the light of the fact that the fast transition to the steady state can eliminate the overshoot, we coercively shortened the effective length of microchannel using a continuous injection of fresh electrolyte through the side microchannels. The effect of the device was confirmed in both visualization and I-V measurements. Conventional micro/nanofluidic device[57] has a cm long microchannel so that it takes 14 hours to get I-V response without overshoot. Using the presenting idea, however, it takes only 2 minutes to obtain the I-V response without overshoot. Considering the repeatability verifications for solid research results (usually 5 times for each 3 different devices), our device can significantly save experimental time and labor.

Chapter 3. The enhancement of ion transport in electroconvection with pulsed electric field

3.1 Introduction

With the rapid development of nanotechnology, various fields using the nanoporous membrane have intensively attracted attention such as desalination, separation, biosensing, and fuel cell. As nanoporous membrane has ion selectivity, cation and anion under electric field have differently moved on the vicinity of the membrane and concentrations at the each side of membrane become distinctively different. Concentration on the anodic side becomes depleted and concentration on the cathodic side becomes enriched. Both regions are called ion depletion zone (IDZ) and ion enrichment zone (IEZ). The phenomenon in which IDZ and IEZ are formed in electrodialysis is called concentration polarization (CP) and in microfluidic chip is called ion concentration polarization (ICP) which is small scale of ED and is affected by electroosmotic flow.

Many researchers have enormously conducted the fundamental studies of CP and ICP from membrane surface science to fluid mechanics [11, 16, 54, 61, 62]. And the measurement of current was the very first thing to do to understand the phenomenon since current was closely related with the mass transfer in the applications. The current-voltage curve of ED has 3 regimes called Ohmic, limiting and overlimiting regimes. The region, which is mainly

used for desalination or separation, is the overlimiting regime, since the mass transfer is most active. And the mass transfer is significantly affected by electroconvection.

Electroconvection (or electroconvective instability) is one of the electrochemical phenomena occurring in the IDZ. The normal electric field causes the IDZ and, under high electric field, extended space charge (ESC) layer is formed. ESC layer is a region where local electrical neutrality is broken down and has a larger number of counter-ion. A small concentration perturbation in the ESC layer is naturally generated and causes the small tangential electric field. From that, counter-ions move, tangential electroosmotic flow occur, and gradient of electrical potential increases. This cycle is repeated and cause fluctuation of concentration, and strong vortex.

Recent studies suggest that the applying pulsed electric field on membrane can enhance mass transport [40, 41, 63-66]. Mishchuk *et al*. have found that the desalination rate was increased when using pulsed electric field compared to applying dc bias under the same average voltage [40, 41, 63]. The antifouling effect due to pulsed electric field was studied by various groups [65, 66]. P.A. Sosa-Fernandeza also showed the enhancement of desalination performance of ED under pulsed electric field by reducing the fouling effect [64].

The studies of current enhancement in pulsed electric field were also conducted by Nikonenko's group and A.I. Schäfer's group [42, 67-69]. They showed that current in the sub-limiting regime was enhanced due to the

restoration of concentration in off state [42, 69]. In the overlimiting regimes, Aminat M. Uzdenova *et al.* showed that the numerical simulation of electroconvection with pulsed electric field using high viscous fluid suggested that the main cause of current enhancement could be diffusion as same as current enhancement in the Ohmic region[67]. S.V.Zyryanova *et al.* experimentally showed that the current enhancement varying frequency [68] and suggested that the increase of current is due to restoration of concentration but the cause of enhancement of current is still discussed.

For optimizing CP and ICP applications to obtain the high desalination rate, it is significantly important to delve into the cause of current enhancement when using pulsed electric field. In this work, we numerically and experimentally investigate the electroconvection in pulsed electric field mode compared to in DC with varying average voltage and frequency in overlimiting regime with electroconvection. We use ICP applications to visualize the motion of fluid. Current was peaked at certain frequency in simulation as same as in experiments. From the simulation, the peak current was obtained because of maintenance of developed convection and was visualized in experiments.

3.2 Materials and Methods

3.2.1 Numerical methods

3.2.1.1 Numerical domain descriptions

The domain of the micro/nanofluidic device could be represented as **Figure 3.1**. The domain was a rectangular which had 4:1 ratio of width and height and the distance from reservoir to ion selective membrane was chosen as a characteristic length. The 2 times much longer width than height was to avoid the spurious numerical results in periodic domain [70]. Domain had three kinds of boundary: Bulk, ion-selective membrane and periodic boundary. The electric field was applied from bulk to ion selective membrane enough to occur ESC layer and only cation could pass through the ion-selective surface. The periodic boundary described that domain had an infinite width. Cation and anion have a monovalent charge and have the same diffusion coefficient (*i.e* KCl electrolyte). Small concentration perturbation was randomly imposed to generate electroconvection.

3.2.1.2 Governing equations and boundary conditions

The simulation was governed by 5 equations: Poisson equation for electric potential, where (c^+- c^-) on the right-hand side is the space charge due to a local imbalance of ionic concentrations, Nernst-Planck equations for transport of monovalent cation and anion, continuity equation for an incompressible fluid, and Navier-Stokes equation with electric body force for momentum transfer of fluid as follows:

$$-\nabla^2\phi = \frac{1}{2\lambda_D{}^2}(c^+ - c^-) \tag{3.1}$$

$$\frac{\partial c^\pm}{\partial t} = -\nabla\cdot(c^\pm\mathbf{u} - \nabla c^\pm \mp c^\pm\nabla\phi) \tag{3.2}$$

$$\nabla\cdot\mathbf{u} = 0 \tag{3.3}$$

$$\frac{1}{Sc}\frac{\partial\mathbf{u}}{\partial t} = -\nabla p + \nabla^2\mathbf{u} - \frac{\kappa}{2\lambda_D{}^2}(c^+ - c^-)\nabla\phi \tag{3.4}$$

The governing equations were nondimensionalized with the diffusion layer thickness L and time, concentration, and electrical potential were respectively nondimensionalized as $t = \tilde{t}/\tau_D$, $c^\pm = \tilde{c}^\pm/c^0$, and $\phi = F\tilde{\phi}/RT$. τ_D is the diffusion relaxation time,

$$\tau_D = \frac{L^2}{D} \tag{3.5}$$

λ_D is the nondimensionalized debye length obtained by dividing the debye length (λ_D) into characteristic length (L), $\lambda_D = \lambda_D / L$. Schmidt number(Sc) and electrohydrodynamic constant(κ) are defined as,

$$Sc = \frac{\mu}{\rho D}, \tag{3.6}$$

$$\kappa = \frac{\varepsilon R^2 T^2}{\mu D F^2}. \tag{3.7}$$

ε is the electrical permittivity of fluid.

All governing equations were fully coupled and were solved using finite element method with boundary conditions in COMSOL multiphysics. At bulk, the dimensionless electrical potential was set to be two kinds of functions. One is a constant function for DC and the other is a rectangular function with a duty cycle of 50% and a zero value in the off state. The average electrical potentials for both functions were set to 40, 60, 80, and 100. The dimensionless frequencies were adopted as 5, 50, 500, 5000, 50000. The dimensionless concentrations of cation and anion were fixed 1 and no-slip boundary condition was adapted. At ion-selective membrane, the dimensionless electrical potential and the dimensionless concentration of cation were respectively Donnan potential, - ln N, and Donnan concentration, N. No flux of anion was considered since anion couldn't pass through the membrane, and no-slip boundary condition was adopted.

We consider Sc = 500 which is Schmidt number of KCl aqueous solution. For κ, N, and ε, typically used value of 5, 2, and 10^{-3}, were adopted. respectively[13, 70, 71].

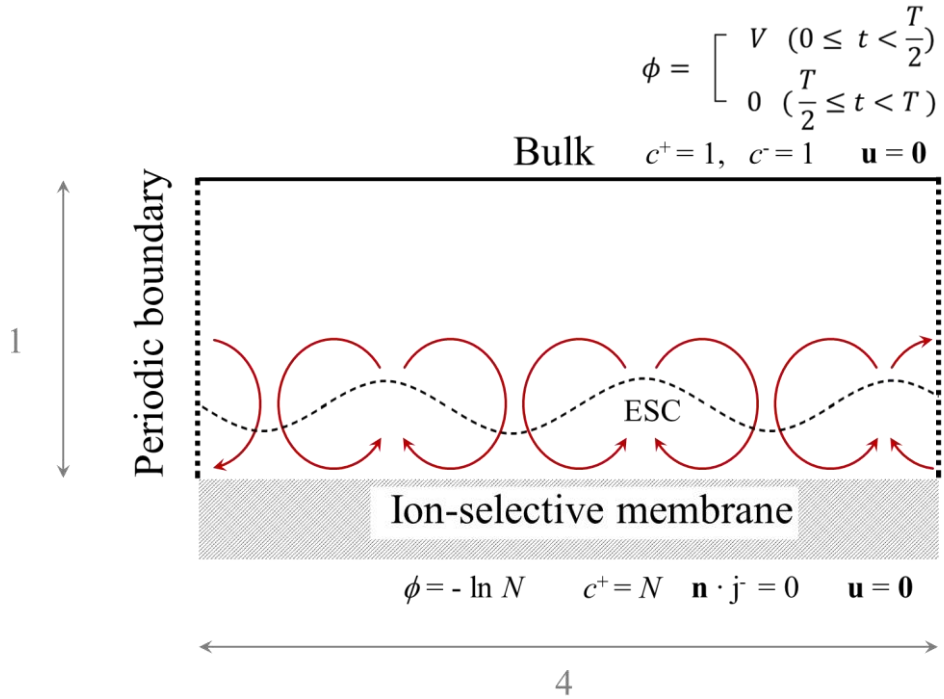

Figure 3.1 Schematic of numerical domain. The characteristic length was the distance from bulk to ion-selective membrane. The rectangular pulse of electrical potential was applied in bulk.

3.2.2 Experimental Methods

Device consisted of microfluidic channel patterning on the PDMS and nanoporous membrane (Nafion sheet). A SU8-2150 film was formed on a wafer using spin coating method. The film was baked at 65 °C for 5 minutes and 95 °C for 20 minutes to evaporate the solvent. After that, the film was exposed to UV through the mask and was baked at 65 °C for 5 minutes and 95 °C for 12 minutes. The coated wafer was immersed in the SU 8 developer w develop microchannels. PDMS mold was formed by pouring the mixture of 10:1 PDMS base and curing agent onto the patterned wafer and heating the mixture at 70 °C for 4 hr. The connection of PDMS microchannel and Nafion sheet proceeded as **Figure 3.2 (a)**. The top of the PDMS mold was cut and Nafion sheet was inserted into the shallow groove. The PDMS cut surface and the Nafion sheet were then bonded using epoxy. The PDMS mold was sequentially attached to the PDMS sheet and slide glass using a plasma bonder and heating at 95 °C. Main- and buffer microchannel shown in **Figure 3.2(b)** had the dimension of 1 mm width, 170 μm depth and 2 mm length with the air valve to refresh the channel [37].

1mM KCL electrolyte was injected and the liquid in side microchannels was cut off using air valve. Ag/AgCl electrode was connected to reservoirs to apply the external voltage. Current was measured at average electrical potential 2.08 V, 2.60 V, 3.12 V and 3.64 V varying frequency (0.0025, 0.025, 0.25, 0.25 and 25 Hz). All measured currents were obtained after at least diffusion relaxation time, 4000 sec.

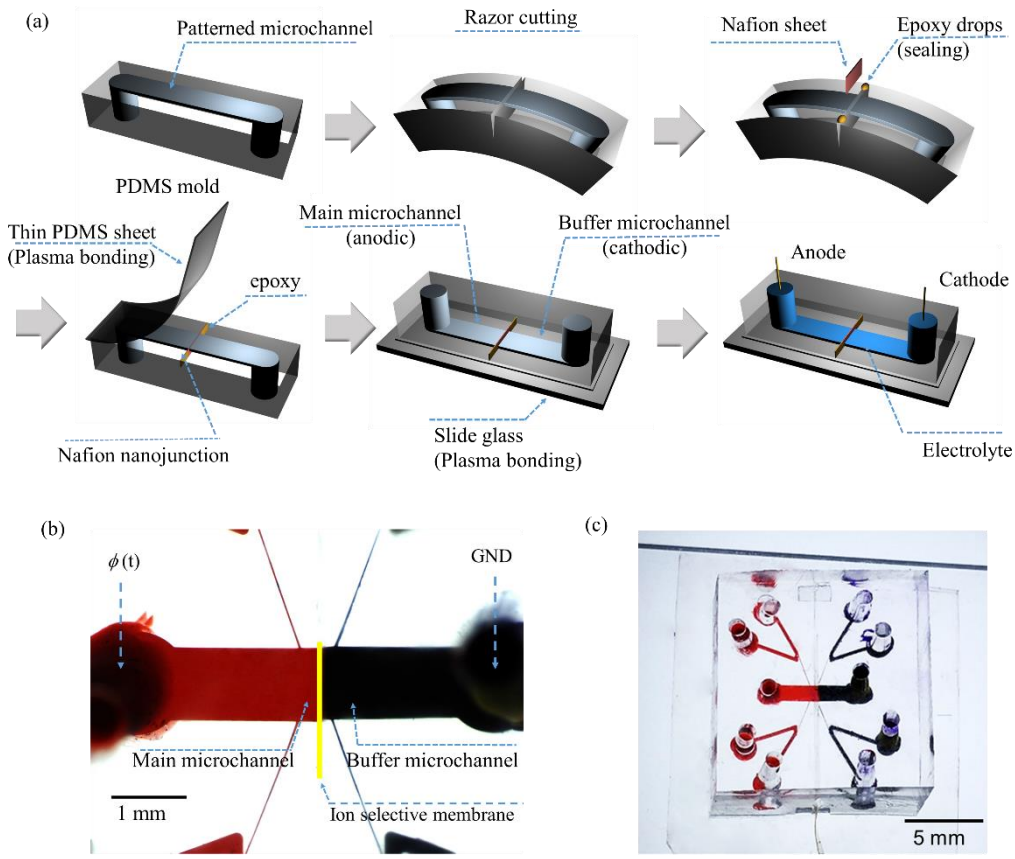

Figure 3.2 (a) Schematic of fabrication method. (b) Schematic of the device. The electrolyte in the side channels was removed by injecting air. (c) Picture of the micro/nanofluidic chip.

3.3 Results

In the numerical simulation, domain had an infinite plane and the electrical potential of bulk was applied with form of rectangular pulse. We calculated the average current density penetrating the membrane to compare with the case of dc bias. The ion flux density on the normal direction of bulk (j_y) and average current density (i_{avg}) was defined as

$$j_y = j_y^{+} - j_y^{-} = (-\frac{dc^{+}}{dy} - c^{+}\frac{d\phi}{dy} + vc^{+}) - (-\frac{dc^{-}}{dy} + c^{-}\frac{d\phi}{dy} + vc^{-}) \qquad (3.7)$$

$$i = \int_{X_{\text{bulk}}} j_y dx \qquad (3.8)$$

$$i_{\text{avg}} = \frac{1}{nT}\int_{nT} i dt \qquad (3.9)$$

j_y^{+} and j_y^{-} are the cation and anion flux density on the normal direction of bulk, v is the flow velocity of y direction, X_{bulk} is the length of bulk in domain, and T is the period of pulsed electrical potential. We obtained quasi-steady state of average current density. The average current density ($i_{avg,\text{dC}}$) under dc bias was also calculated from

$$i_{avg,dc} = \frac{1}{t_2 - t_1}\int_{t_1}^{t_2} i dt \qquad (3.10)$$

, since the current was fluctuated due to electroconvection. t_1 and t_2 are the

time in the quasi-steady state.

In **Figure 3.3 (a),** we compared the average current density in pulsed electrical field and dc bias, $i_{avg}/i_{avg,dc}$. The average current density enhancement ratio increased as the frequency of electrical potential increased from $f = 5$ to $f = 5000$, and was peaked at $f = 5000$. After $f = 5000$, the ratio decreased.

We also certified the same tendency in experiments (**Figure 3.3 (b)**). Current was measured and was divided by surface area of membrane to obtain current density. Average current density was calculated by (3.9) and (3.10). The frequencies in experiments were nondimensionalized as $f = 5$, 50, 500, 5000 and 50000. Experimental values were also optimized at $f = 5000$. The enhancement ratios of numerical simulation and experiments have differences and it would be discussed next chapter.

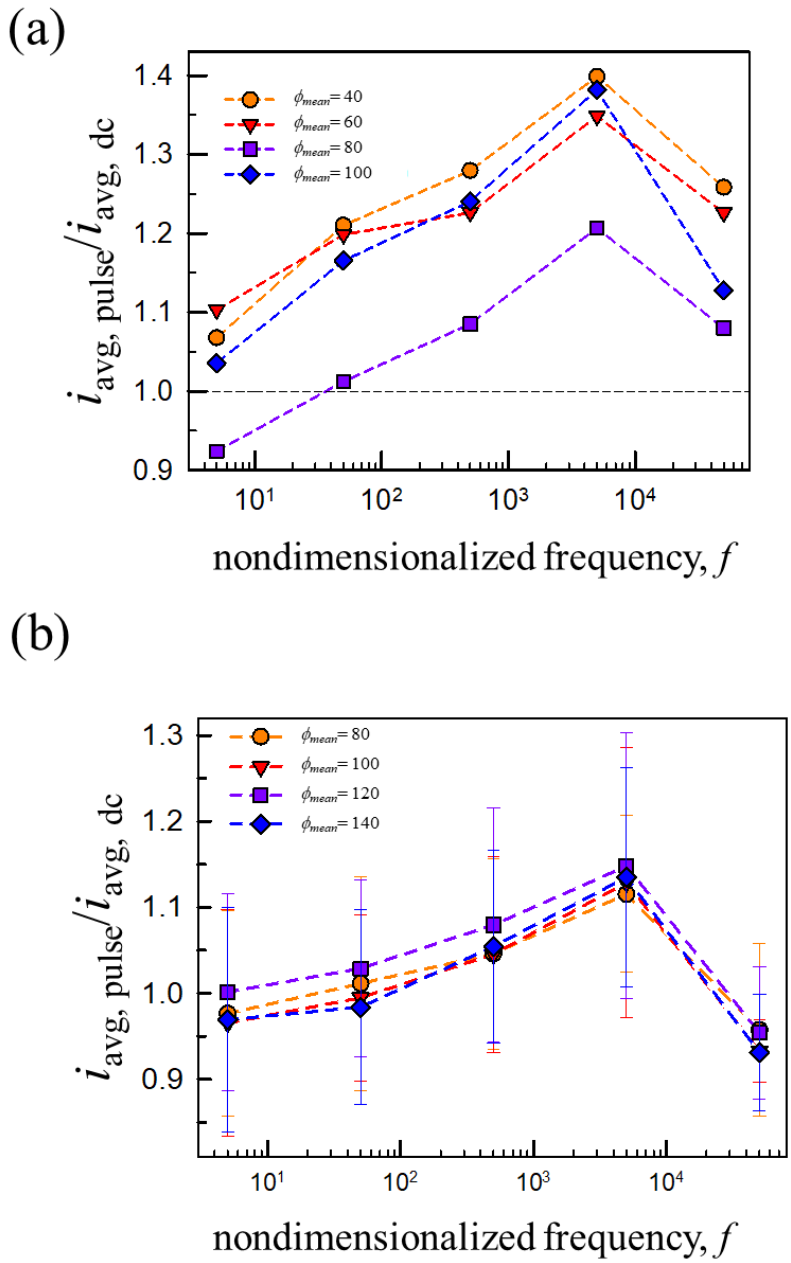

Figure 3.3 The average current density enhancement ratio in pulsed electric field ($i_{avg,\ pulse}$) compared to in dc bias ($i_{avg,dc}$) according to nondimensionalized frequency, f (a)in numerical simulation, and (b)in experiments. Both graph has a same tendency and peak current.

3.4 Discussions

3.4.1 Concentration restoration effect on current density

The average concentration profile under the pulsed electric field could be obtained from the simulation (**Figure 3.4 (a)**). Concentration was significantly fluctuated in low frequency, f = 5. However, the difference between the concentration of on state and off state was almost diminished in high frequency, f = 5000. As the time of off state became short, the ions couldn't diffuse and the concentration was not fluctuated.

We could find the restoration effect from diffusion in current density as **Figure 3.4 (b)**. The current density of on state always started at high value and reduced since increased concentration in ion depletion zone during off state enhanced the electrical conductivity.

As concentration fluctuation was almost diminished, the current path was also maintained as **Figure 3.4 (c)**. In experiments, the concentration was indirectly obtained by SRB and 40 nm carbon particles. And we also obtained concentration profile from numerical simulation. The concentration profile was binarized at the value of 1/4.

At the low frequency, the electroconvection was formed in on state, however the concentration was restored in off state. Therefore, the electroconvection was reinitiated and current path was constructed and destructed repeatedly.

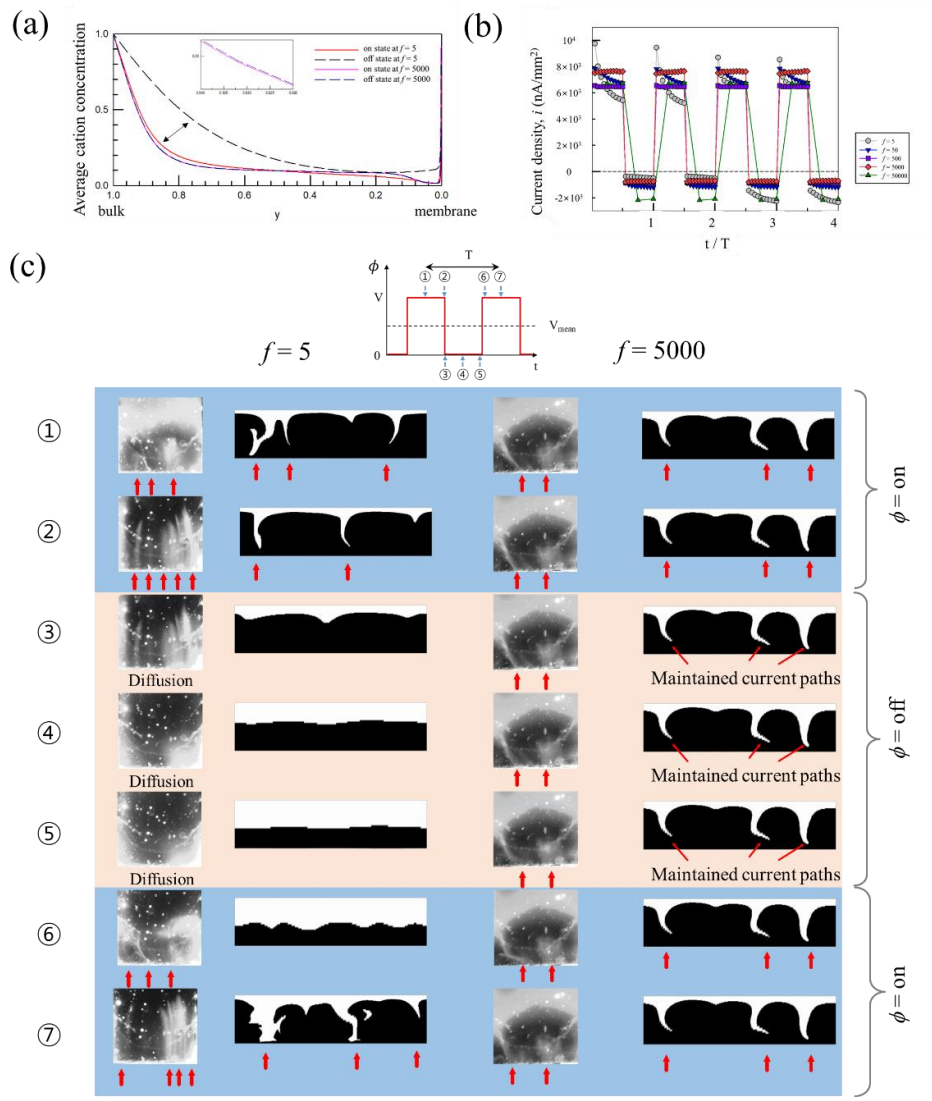

Figure 3.4 (a) Current density according to normalized t / T in experiments. (b) Average concentration profile at $f = 5$, and $f = 5000$ according to the distance from membrane to bulk in numerical simulation. At low frequency, the concentration was largely fluctuated while the similar concentrations were obtained at high frequency. (c) Concentration profile obtained from experiments and numerical simulation at $f = 5$ and $f = 5000$. In the simulation, the figure of concentration was binarized at c = 1/4. White and

black regions are high and low concentration region, respectively. Electroconvection was regenerated in low frequency while current path was maintained in high frequency.

At the high frequency, the electroconvection was generated slowly in on state. But the current path was maintained in off state and didn't dispersed as **Figure 3.4 (c)**. As a result, the current density of on state was a constant, not reducing, due to maintenance of current path.

3.4.2 Convection retardation effect on current density

The retardation time and magnitude of convection was calculated to discuss the results in details. The current density was related with the ion flux density as equation (3.8) and ion flux is derived from diffusion, drift, and convection. The boundary condition of electrical potential was consecutively changed in our system, so the retardation time of each component in ion flux density equation should be considered.

In our numerical simulation, the nondimensionalized time is based on the diffusion relaxation time. The diffusion relaxation time is the value of 1 in our system. The relaxation time of drift is $O(10^{-4})$ [8]. Therefore, the effect of retardation from drift would be negligible in our system. And the relaxation time of convection ($\tilde{\tau}_{conv}$) of whole domain could be expressed as

$$\tilde{\tau}_{\mathrm{conv}} = \frac{\rho L^2}{\mu}. \tag{3.11}$$

Nondimensionalized convection relaxation time (τ_{conv}) was obtained by

$$\tau_{\mathrm{conv}} = \frac{\tilde{\tau}_{\mathrm{conv}}}{\tau_{\mathrm{D}}} = \frac{1}{\mathrm{Sc}}. \tag{3.12}$$

From (3.12), $\tau_{conv} = 2 \cdot 10^{-3}$ in numerical simulation. It means that the required time to reach final velocity is $2 \cdot 10^{-3}$.

We could find the τ_{conv} in experiments. Injecting the emulsion of 1 mM KCl and oleic acid oil with the volume ratio of 100:1 to the microchannel, convection relaxation time was obtained. The motion of oil droplet was

transited to brownian motion after at least 6 sec. The convection relaxation time in experiments would be $O(1)$-$O(10)$ sec. The nondimensionalized convection relaxation time was calculated as $O(10^{-3})$-$O(10^{-4})$. So the enhancement of average current density would be similar as numerical simulation.

The change of convection was also certified from the numerical simulation and experiments. In numerical simulation, the magnitude of whole convection was indirectly quantified from root-mean-square of flow velocity (v_{rms}). The v_{rms} is defined as

$$v_{\mathrm{rms}} = \frac{1}{\mathrm{A}} \int_{\mathrm{A}} \sqrt{(u^2 + v^2)} d\mathrm{A} \tag{3.13}$$

u is the flow velocity of x direction, and A is the surface area of domain. The change of v_{rms} in 1 pulse was calculated as **Figure 3.5 (a).** And the average of v_{rms} in pulses was defined as

$$v_{\mathrm{avgrms}} = \frac{1}{nT} \int_{nT} v_{\mathrm{rms}} dt \tag{3.14}$$

and the v_{avgrms} ratio was obtained as **Figure 3.5 (b)**.

In Figure 3.5(b), the v_{avgrms} ratio was weakly increase as frequency increase until $f = 500$. However, after the $f = 5000$, we could obtain that v_{avgrms} ratio was strongly reduced.

The current density enhancement can be explained considering concentration distribution, magnitude of flow in whole channel and the retardation effect of diffusion and convection. At the low frequency, $f = 5$, and

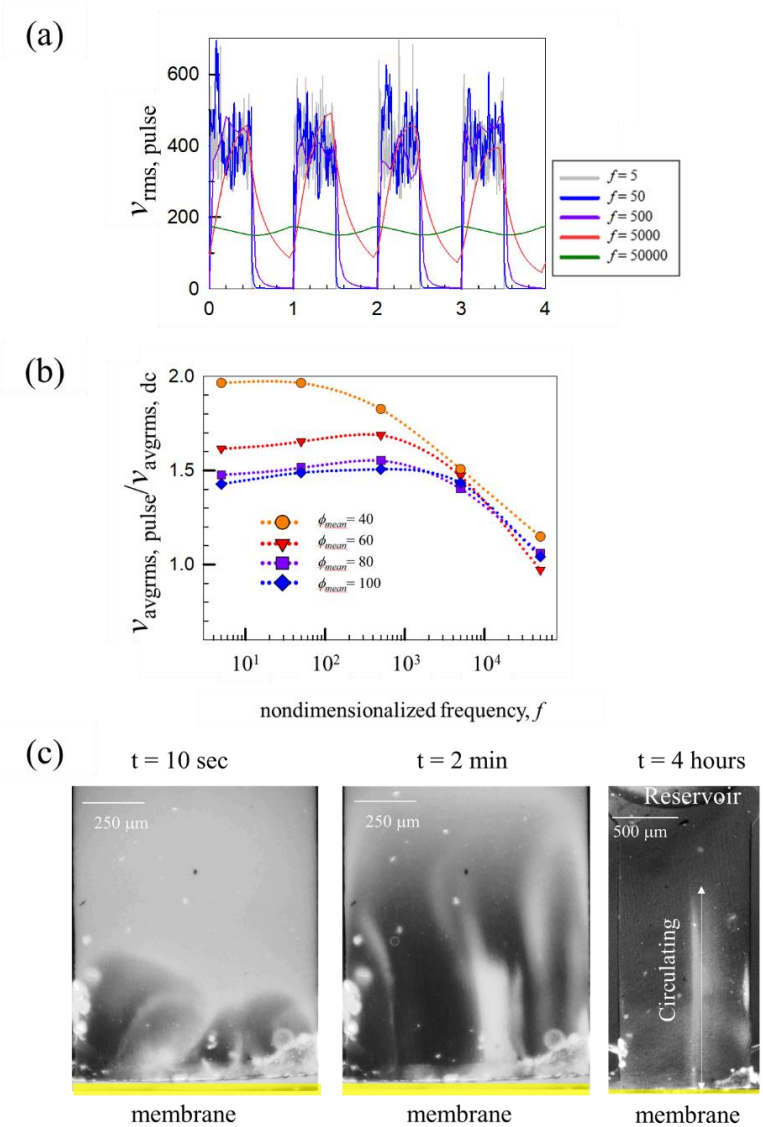

Figure 3.5 (a) Root mean square of velocity in whole domain according to time. Remnant convection was exist at f = 5000 and 5000. (b) Average root mean square of velocity with pulsed electric field compared to with dc bias according to nondimensionalized frequency. The ratio was peaked at f = 500 and reduced. (c) Picture of particle in f = 5000. Developed vortex represent the remnant convection in off state even if the particle was discontinuously moved. Particle had 40 nm diameter.

50 electroconvection in on state would be similar with in dc bias. The retardation effect would be neglected and the ion flux is determined by drift and convection. Since we applied twice electrical potential of the dc bias, the current density in on state would be higher than in dc bias of same average electrical potential. In the off state, the convection of the whole microchannel was diminished as **Figure 3.5 (a)** and the concentration change was largely affected by diffusion. Therefore, the ions were only influenced by diffusion in off state. The back current was found in experiments as **Figure 3.4 (b)**. The ion enrichment zone has a higher concentration than ion depletion zone and ions were moved to the ion depletion zone through the membrane. As a result, the large back current was measured. The back current was compensated for high value of current density at transition point from off to on. Therefore, the current density in low frequency was almost same as under dc bias. The numerical simulation didn't have an ion enrichment zone that the back current was weak and total average current density was enhanced compared to current density under dc bias.

As the frequency became faster, average current density became higher. The off time of pulse was short and the restoration effect was reduced. The back current was also reduced as **Figure 3.4 (b)**. Instead, from the **Figure 3.5 (a),** the convection in off state was remnant.

When the nondimensionalized frequency was 5000, the average current density has an optimal point. The diffusion in off state was negligible however the convection was remnant as **Figure 3.5 (a)**. Convection was found in

experiments (**Figure 3.5 (c)**). When the pulse was applied, the electroconvection was generated in on state. The particle moved and stopped repeatedly. However, the particles were followed the same convection like as the convection didn't disappear. The long convection was developed after 4 hours as **Figure 3.5 (c)**. The particle slowly circulated along the convection even if the particle couldn't circulate the one cycle in a pulse. We could guess that the convection in off state was too small that the drag force couldn't move the particle, however, the convection existed. Considering the convection retardation time was $O(10^{-3})$-$O(10^{-4})$, the convection can be existed. Therefore, the electroconvection was maintained and high flow velocity was kept in whole channel. Therefore, the ion flux was enhanced and average current density was peaked.

After the optimal point, the current density became shrunk at $f = 50000$. The remnant convection was existed, however the convection induced from electroconvection was weak as **Figure 3.5 (a)** and **(b)**. Therefore the ion flux was reduced and current density decrease.

3.5 Conclusion

We observed the average current density enhancement of electroconvection with pulsed electric field compared to with constant voltage. The average current density according to frequency had an optimal current density in numerical simulation and experiments. The change of concentration distribution in pulse was calculated in numerical simulation and certified the maintained current path in experiments. The big concentration variation in low frequency increased the electrical conductivity, but the restoration effect had a small influence on the average current density. At the optimal frequency, concentrations in on and off state had negligible difference and the current path was maintained. We also verified that the retardation of convection would strongly affect the ion transport. As the frequency was high, the convection didn't disappear in off state and remnant convection maintained the fast transport of ions. Electroconvection was continuously developed and maintained even if electrical potential was in off state in the middle. After the optimal point, average current density was shrunk since the convection was undeveloped in high frequency. From this work, the transport of ions in electroconvection could be enhanced considering the retardation time of convection and frequency, however, the in-depth study of convection was required.

Chapter 4. Conclusion

In this work, we studied the transient state of ion concentration polarization. One is overshoot current occurring between the Ohmic regime and limiting regime. The overshoot current was often observed in ICP applications such as separator, desalination, and biosensor. Such kind of ICP separator needed the accurate current–voltage curve due to the variation of ion depletion zone. Overshoot current was relevant with the transient state of concentration in diffusion layer. The overshoot current could be controlled by varying the effective length of microchannel and the sweep rate of the voltage. We certified the generation of overshoot is determined by diffuse relaxation time, $\tau_{D,}$ as well known. We suggest the noble device in micro/nanofluidic chip.

Second, we continuously changed the boundary condition of electrical potential using pulse. Applying pulsed electric field on electroconvection has various advantage such as reducing the water split, fouling effect on membrane and the current enhancement. However, the cause of current enhancement was still unclear. We verified current enhancement in numerical simulation and experiments. At the same average electrical potential, the current density of pulsed electric field was higher than the current density of constant voltage. Their current density enhancement was due to convection, not restoration. We certified the change of concentration profile in numerical

simulation and verified the diffusion was negligible in high frequency in experiments. Restoration effect was minimal, however the remnant convection enhance the ion flux and increase the current density. The remnant convection was certified in simulation and experiments .Even more, average current density was reduced at high frequency since the short time of on state generated undeveloped electroconvection.

Investigation of ICP in transient state was critical issue because the applications were always operated at fluctuating circumstance. We experimentally studied the ICP focusing on current-voltage characteristic. Moreover, the electroconvection one of the critical issues in ICP phenomenon was studied and discussed. From the thesis, the part of the perm-selective transport phenomena in transient state was verified and the perm-selective application, especially focused on the ion transport through the membrane such as desalination device or separator, would be enhanced.

Appendix

A. The 1-D simulation of Ion Concentration Polarization in dead-end Channel

We obtained the spaciotemporal change of c^+ for different efficient microchannel length, L_{eff} by solving 1-D numerical simulation of the Poisson equation and Nernst-Planck equation as follows.

$$\varepsilon\nabla^2\phi = zF(c_+ - c_-) \quad \text{and} \quad \frac{\partial c_\pm}{\partial t} = -\nabla\cdot(-D_\pm\nabla c_\pm \mp \frac{FD_\pm}{RT}c_\pm\nabla\phi).$$

where ε is the electric permittivity of water, ϕ is the voltage, z is the ion valence for symmetric electrolyte, F is the faraday constant, c^+ and c^- are cation and anion concentrations, t is the time, $D_\pm$ is the diffusivity of each ion, R is the gas constant, and T is the temperature. The numerical calculation were carried using COMSOL multiphysics 4.4. Boundary conditions were (i) bulk electrolyte concentration and linearly increasing voltage at the bullk and (ii) the Donnan potential and the Donnan concentration for cation, no-flux condition for anion at the nanojunction. The length scale was nondimensionalized with L = 100 μm so that the nanojunction and the bulk were located at x = 0 and x = 10, respectively. A constraint of "bulk concentration" was additionally assigned at L_{eff}/L where a fresh solution was injected through the side microchannel. The sweep rate of voltage was 0.05 V / 10 sec.

When L_{eff} was 500 μm and 750 μm, diffusion layer was fully extended

to side channel before reaching limiting current regime. In other word, the concentration gradient became constant (black straight lines) at V = 0.31 V and 0.47 V, respectively as small arrows indicated. However, when L_{eff} were 1000 μm, the diffusion layer continuously expanded and stopped to form a constant gradient at V = 0.93 V which laid in overlimiting current regime. Thus, obtaining linear concentration (*i.e.* reach steady state) also required more time as L_{eff} increased. Furthermore, since the ion depletion zone was confined in the vicinity of nanojunction as shown in the inset of **Figure A.1**, the ion transportation solely depended on this constant concentration gradient so that the diffusive transportation would play a deterministic role for I-V characteristic.

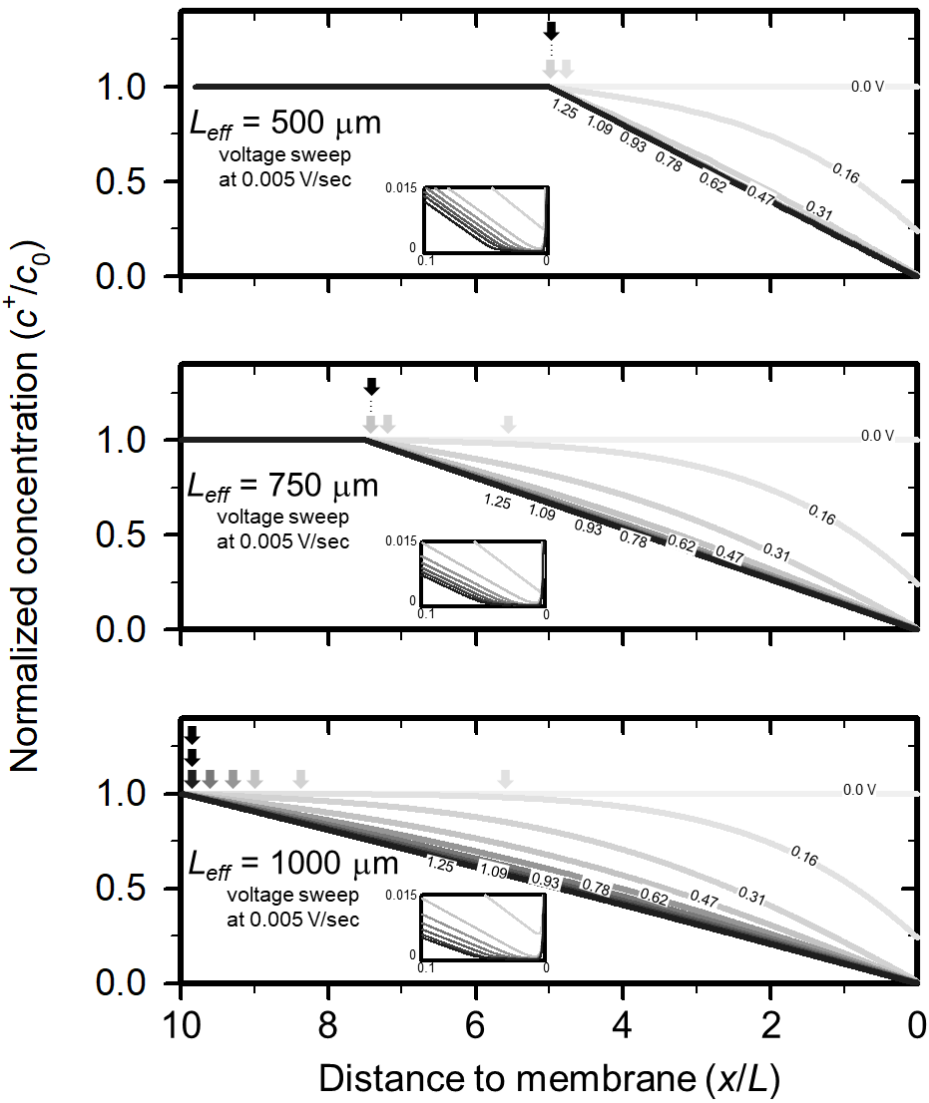

Figure A.1 Spatiotemporal cation concentration profile for different efficient microchannel length, L_{eff} = 500, 750, and 1000 μm. Left is reservoir and right is membrane.

B. Investigation of overlimiting current in confined microchannel by hydraulic convection.

B.1 Convergence of overlimiting current

As the sweep rate of voltage increase, the current-voltage curve had a overshoot current and entranced the overlimiting regime. **Figure 2.4** showed that the current was converged in limiting regime. We also verified that the overlimiting regime was also converged as Figure B. 1. The same device in Chapter 2 was used and effective length of microchannel was 500 μm. We varied the sweep rate of voltage from 0.05 V / 0.3 sec to 0.05 V / 30 sec. In this device, diffusion relaxation time is 250 sec. The sweep rate 0.05 V/ 0.3 sec reached steady state at 0.45 V. Therefore, the overshoot current was absent. However, the pink line reached steady state at 2.2 V, 130 sec and the cyan line entered the steady state at 5 V, 100 sec. Even if the overshoot current was observed and limiting current was measured higher, the current would be converged after enough time. Different thing with Chapter 2 is that the required time to reach steady state was shorter than the diffusion relaxation time. As the voltage quickly increase, the drift of ion in diffuse layer was enhanced. The diffuse layer in overlimiting regime was shrink because of expansion of ion depletion zone. Therefore, the required time would be reduced.

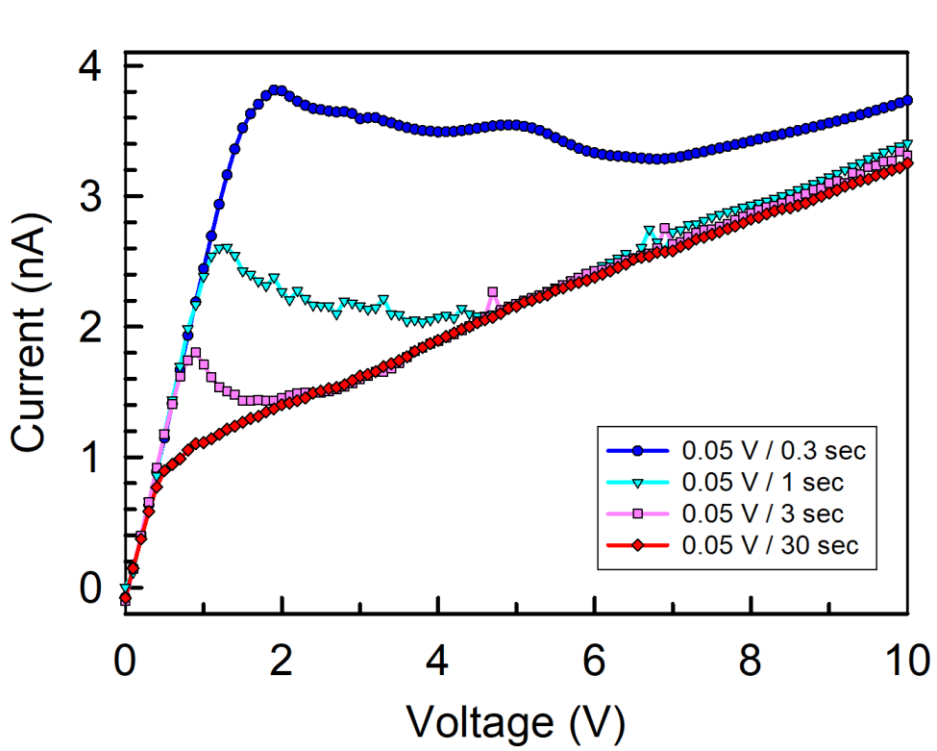

Figure B.1 current-voltage characteristic with overshoot current. Current was converged in overlimiting regime even if the sweep rate of voltage was enough high.

B.2 verification of regime shift in overlimiting current

From the **Figure 2.2**, overlimiting conductance (OLC) was obtained. Dydek et al. suggested that the overlimiting conductance was relevant with length of microchannel (L). The equations of OLC according to L is different in surface chare regime and electroosmotic flow regime [6]. In the surface charge regime, the OLC was proportional to L^{-1}. And the OLC was proportional to $L^{-1.8}$ in electroosmotic flow regime. In our work, we obtained OLC from L= 150 μm to 2000 μm. The depths of all the microchannels were 15 μm, which normally had electroosmotic flow regime, however, the OLC followed the equation of SC in short microchannel. The diffuse layer was fluctuated by hydraulic convection in short microchannel and the hydraulic convection enhanced the convection and ion transport in ion depletion zone.

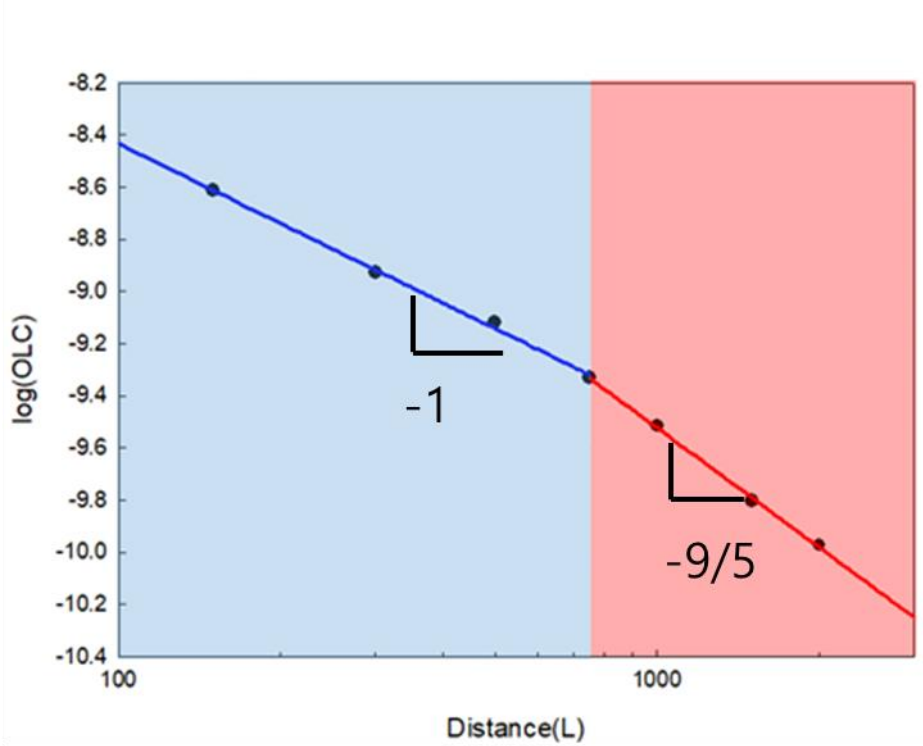

Figure B.2 overlimiting conductance according to length of microchannel.

C. Removal of Oil Droplet from Emulsion using Micro/Nanofluidic chip

C.1 Introduction

After the industrial revolution, accidental oil spill has occurred several times such as Gulf war oil spill in 1991, Maxico oil spill in 2010, and Ixtoc 1 oil well in 1979. Spilled oil on the ocean are waved, are divided into small oil droplets which have the diameter under 70 μm and the oil droplets are dispersed [72-75]. The part of oil droplets are biodegraded [74, 75], however remnant oil droplets are absorbed or attached in fishes and animals. Even though there is the small amount of oils, oil pollution causes serious disturbance of the ecosystem, animal disorders and adversely affects humans through the food chain. Therefore, various field such as chemical engineering [76-78], material engineering [79-81], and microfluidics [25, 82] have intensively focused to solve the oil contamination.

In microfluidics, there were several researches for oil droplet separator [83, 84]. Goet *et al* separated the oil using isotachophoresis [83], Carlo *et al* manipulate and ordered the oil droplets using inertia focusing [84], and Kim *et al* purified water from emulsion using ion concentration polarization (ICP) devices.

ICP is the electrochemical phenomena generating near the nanoporous membrane when the electric field is applied through the membrane. The concentration was depleted on the edge of the membrane and was enriched

on the other edge of the membrane. Each regions is called ion depletion zone and ion enrichment zone, respectively. Since electric field is the very enhanced near the ion depletion zone, charged species are pushed away from the ion depletion zone.

In this work, we fabricated micro/nanofluidic devices for separating diverse oil droplets. The devices generated ICP for separating oil from emulsion. We measured the oil removal efficiency using image processing. In the limiting current regime, oil removal efficiency was peaked and oil droplets were clogged at the high external voltage. Comparing the properties of oil droplets, we suggest that the dielectrophoretic force have a major effect on the movement of oil droplets near ion depletion zone. The diameter of oil droplet is the critical factor of oil removal efficiency.

C.2 Experimental setup

The schematic diagram of devices is shown in **Figure C.1**. The microfluidic channels were fabricated from polydimethyl-siloxane (PDMS) using soft lithography fabrication. To generate ion concentration polarization, Nafion (Sigma Aldrich, USA) was used as the nanoporous membrane using surface patterning method [57]. The main channel was divided into two channels. One was preconcentrated channel where the oil droplet was gathered and the other was purified channel where the oil droplets were removed.

We use 5 kinds of oil: Oleic acid, Silicone oil AR 20(Polyphenyl-methylsiloxane, Sigma-Aldrich, USA), canola oil, decane, isoocatane. Each emulsion solutions had 1:100 volume ratio of oil and aqueous solution (1 mM KCl). Emulsion was formed by ultra-sonication (40 kHz) and the size of oil droplets were under 5 μm. The emulsion was injected to separating channel and 1 mM KCl solution was injected to buffer channel.

Images of manipulating oil droplets were captured by an inverted fluorescent microscope (IX53, Olympus) and CellSens program. Pressure was driven by gravitational force derived from the difference of height in reservoir connected to 1 mL pipet tip. Because a fluid velocity driven by gravity was 0.78 ± 0.01 nL/s derived from observed particle velocity 520 ± 5 μm/s. The height of solution in pipet tip was negligibly reduced, so volume velocity was kept.

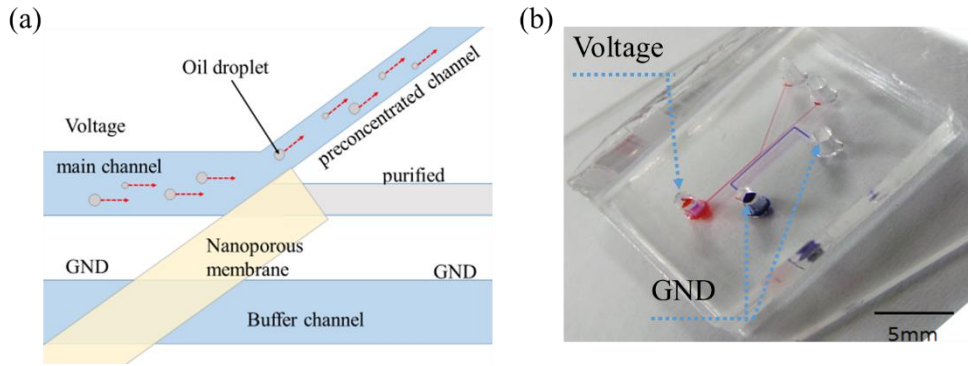

Figure C.1 (a) Schematic of device, electric field was applied from reservoir of main microchannel to buffer channel. Hydraulic pressure is derived using difference of height of solution in reservoir. (b) Picture of the devices.

Oil removal efficiency was quantified using image processing (MATLAb) as **Figure C.2**. The depth of microchannel, 15 μm, was enough shallow to capture the most of the oil drop. Microchannel was recorded and two parts of image was cropped. One is injected microchannel (area A in **Figure C.2**) and the other is purified channel (area B in **Figure C.2**). Cropped images were binarized and were used to calculate the oil density in microchannels. Oil density (ρ) was defined as sum of oil surface area divided by captured area. Oil removal efficiency was defined as $1-\rho_A/\rho_B$, ρ_A is oil density in area A and ρ_B is oil density in area B.

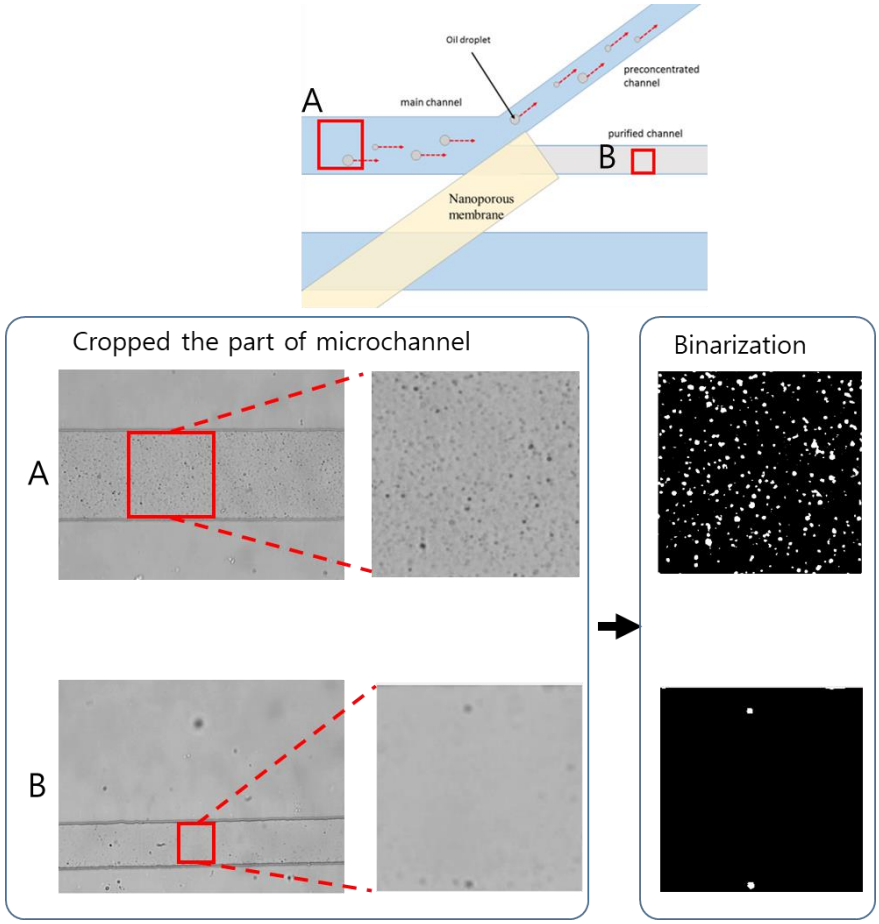

Figure C.2 Image processing method of oil removal efficiency. Micro channel was captured at injecting part and purified part. The image was binarized and sum the white area.

C.3 Results and discussion

ICP devices were performed with varying voltage. With applying voltage ion depletion zone was formed and expanded. Oil droplet was pushed away from ion depletion zone since high electric field was generated near the ion depletion zone[29] (**Figure C.3 (a)-(e)**). Oil droplet was gradually pushed up from Nafion with expansion of ion depletion zone and, finally, all the oil droplet was moved to the preconcentrated channel. However, when voltage is upper 48 V, oil droplets were plugged in main channel as **Figure C.3 (e)**.

Oil removal efficiency of oleic acid and silicone oil was calculated with varying voltage (**Figure C.3 (f)**). From **Figure C.3 (g)**, the current-voltage curve was in Ohmic regime under 32 V. Therefore, we can know that the boundary of diffuse layer was being in contact with the Nafion. Therefore, ion depletion zone was formed but was not covered throughout the entrance of the purified channel, and oil droplet could move to purified channel. The ion depletion zone was expand enough to fully cover the entrance of purified channel, the slope of current became constant as red area in **Figure C.3 (g)**. All the oil droplet in the vicinity of Nafion was repelled from the Nafion and move to the preconcentrated channel. Therefore, the peak removal efficiencies were obtained at 32 V. However, oil removal efficiency decreased when the voltage was upper 36 V. Submicron oil droplets were leaked and most of them were pass the ion depletion zone along the microchannel wall where the flow is fast because

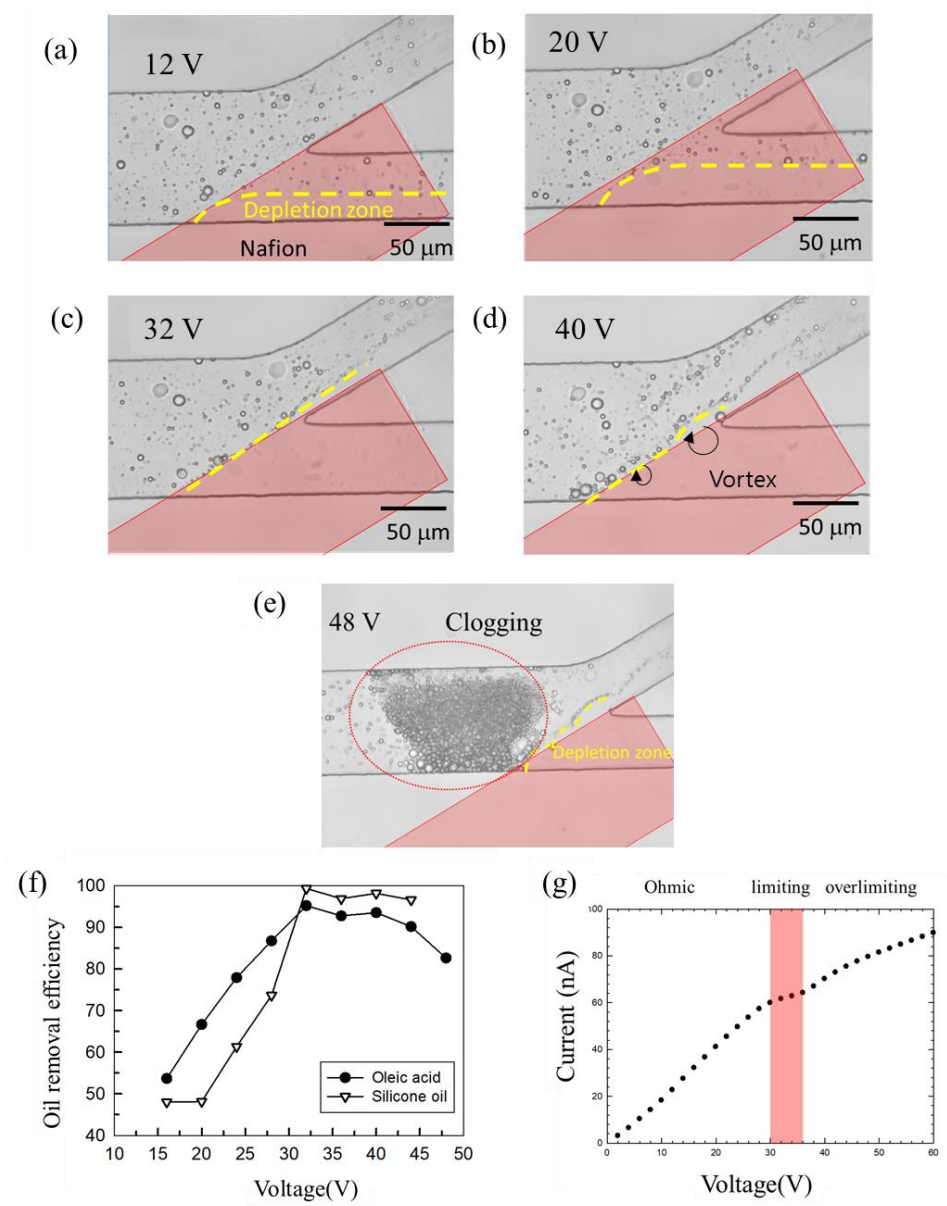

Figure C.3 (a)-(e) the picture of the oil removal according to voltage 12, 20, 32, 40, 48 V. Main channel was clogged in (e). (f) Oil removal efficiency of oleic aiccd and silicone oil droplet according to voltage. (g) Current-voltage curve of the devices.

of second kind of electroosmotic flow[29, 85]. Upper 48 V, the vortex generated by ion depletion zone trapped oil droplets and eventually plugged the main channels.

As peak oil removal efficiency was obtained at the same voltage, 32 V, we additionally measured oil removal efficiency of the other oils as **Table C.1**. We thought that oil droplets were influenced by drag force ($\mathbf{F}_D$), electrophoretic force ($\mathbf{F}_{EP}$), and dielectrophoretic force ($\mathbf{F}_{DEP}$) as the Jeon's work [23]. So sum of the forces was,

$$\sum \mathbf{F} = \mathbf{F}_D + \mathbf{F}_{EP} + \mathbf{F}_{DEP} \tag{B.1}$$

We assumed that the oil droplets were sphere particle. Then,

$$\mathbf{F}_D = -6\pi\mu a(\mathbf{u}_p - \mathbf{u}_f) \tag{B.2}$$

$$\mathbf{F}_E = 6\pi\zeta_p\varepsilon a\mathbf{E} \tag{B.3}$$

$$\mathbf{F}_{DEP} = -2\pi\varepsilon a^3\mathbf{E}\bullet\nabla\mathbf{E} \tag{B.4}$$

,μ is the viscosity of fluid and and a is the diameter of the oil droplet, $\mathbf{u}_p$, $\mathbf{u}_f$ is the velocity of paricle and fluid, respectively. ζ_p is the zeta potential of particle and ε is the dielectric constant of fluid. Oil repulsion from the ion depletion zone was determined by electrophoresis and dielectrophoresis. If the electrophoresis is dominant, the oil removal efficiency of decane and isooctane should higher than oleic acid, silicone oil, and canola oil. However, the opposite results were obtained. The results showed that the diameter was significant factor of oil removal efficiency. The oil droplets with upper 1 μm diameter was more efficiently removed than submicron oil

droplet. We could thought that zeta potential was influenced by particle size :small particles have small zeta potential[75]. But in the case of oil droplet, the zeta potential could be reduced as the diameter became smaller [86-88], so it would be hard to say that the electrophoresis determine the movement of oil droplets. From the equation (B.4), small particles were less affected by dielectrophoretic forces. And this scenario can explain the leakage of oil as we mentioned above. At the interface of microchannel wall and Nafion, there was the amplified electroosmotic flow was generated since the electroosmotic flow in the ion depletion zone was proportion to $\mathbf{E}^2$ [29, 85]. As drag forces were enhanced and dielectric forces less affected the small droplets, the small droplets were leaked.

	Oleic acid	Silicone oil	Canola oil	Decane	Isooctane
Viscosity [mPa· s]	27.64	1.01	54	0.92	0.473
Dielectric constant	2.5	2.5	3.1	2.0	1.94
Diameter ($2\bar{r}$)	1.03 ± 0.47	2.91 ± 2.80	2.40 ± 2.24	0.77 ± 0.33	0.74 ± 0.29
average zeta potential (mV)	-25.28	-24.25	-34.25	-50	-50
Oil Removal Efficiency (%)	95~97	97~99	95~97	80~86	75~80

Table C.1 The properties of oil droplets. Viscosity, diameter, zeta potential was measured. Dielectric constant was referenced [89-93]. Viscosity, diameter and zeta potential of oil droplets were measured. Oil removal efficiencies were measured at 32 V.

C.4 Conclusion

In this work, we measured the oil removal efficiencies of oil droplets varying external voltage. In the limiting regime, there was no vortex and ion depletion zone fully covered the entrance of purified channel. Therefore, upper 95 % of oil droplets were removed. In the high external voltage, vortexes were generated and finally clogged the main channel. And we suggested that the main factor of repulsion of oil from ion depletion zone was dielectrophoresis since the oil removal efficiency was determined by the diameter of oil droplets.

The device for the seperation of oil in labortary could be useful and also it could be applied on the biodiesel extractor as **Figure C.4**. Using the vortex generated by ion depletion zone in overlimiting regime, algae cell could be shredded and oil could be preconcentrated at the same time.

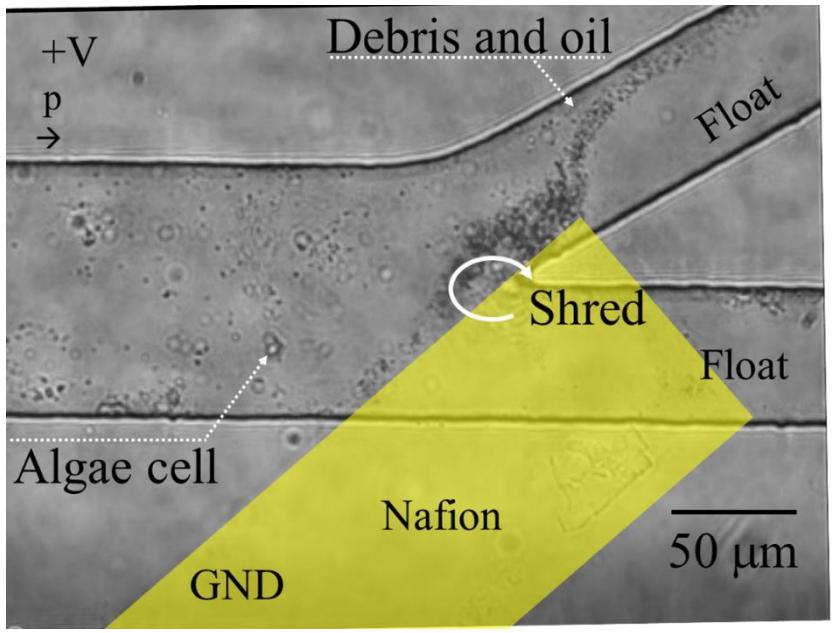

Figure C.4 picture of extraction of biodiesel from algae cells. Algae cell was shredded by high speed vortex and move to the preconcentrated channel.

Bibliography

[1] J. H. B. Masliya, Subir., *Electrokinetic and colloid transport phenomena,* 2006. John Wiley & Sons

[2] D. Stein, M. Kruithof, and C. Dekker, "Surface-Charge-Governed Ion Transport in Nanofluidic Channels," *Physical Review Letters,* vol. 93, no. 3, p. 035901, 07/15/ 2004.

[3] M. N. Szentirmay and C. R. Martin, "Ion-exchange selectivity of Nafion films on electrode surfaces," *Analytical Chemistry,* vol. 56, no. 11, pp. 1898-1902, 1984/08/01 1984.

[4] A. Lindheimer, J. Molenat, and C. Gavach, "A study of the superselectivity of Nafion perfluorosulfonic membranes," *Journal of Electroanalytical Chemistry and Interfacial Electrochemistry,* vol. 216, no. 1, pp. 71-88, 1987/09/01/ 1987.

[5] S. J. Kim, Y.-C. Wang, J. H. Lee, H. Jang, and J. Han, "Concentration Polarization and Nonlinear Electrokinetic Flow near Nanofluidic Channel," *Physical Review Letters,* vol. 99, p. 044501, 27 Jul 2007 2007.

[6] E. V. Dydek, B. Zaltzman, I. Rubinstein, D. S. Deng, A. Mani, and M. Z. Bazant, "Overlimiting Current in a Microchannel," *Physical Review Letters,* vol. 107, p. 118301, 2011.

[7] S. Nam *et al.*, "Experimental Verification of Overlimiting Current by Surface Conduction and Electro-Osmotic Flow in Microchannels," *Physical Review Letters,* vol. 114, no. 11, p. 114501, 2015.

[8] C. L. Druzgalski, M. B. Andersen, and A. Mani, "Direct numerical simulation of electroconvective instability and hydrodynamic chaos near an ion-selective surface," *Physics of Fluids,* vol. 25, no. 11, p. 110804, 2013/11/01 2013.

[9] I. Rubinstein and B. Zaltzman, "Extended space charge in concentration polarization," *Advances in Colloid and Interface Science,* vol. 159, no. 2, pp. 117-129, 2010.

[10] I. Rubinstein, "Mechanism for an electrodiffusional instability in concentration polarization," *Journal of the Chemical Society, Faraday Transactions 2: Molecular and Chemical Physics,* 10.1039/F29817701595 vol. 77, no. 9, pp. 1595-1609, 1981.

[11] I. Rubinstein, B. Zaltzman, and I. Lerman, "Electroconvective instability in concentration polarization and nonequilibrium electro-osmotic slip," *Physical Review E,* vol. 72, no. 1, p. 011505, 07/21/ 2005.

[12] S. M. Rubinstein *et al.*, "Direct Observation of a Nonequilibrium Electro-Osmotic Instability " *Physical Review Letters,* vol. 101, p. 236101, 2008.

[13] A. S. Khair, "Concentration polarization and second-kind electrokinetic instability at an ion-selective surface admitting normal flow," vol. 23, no. 7, p. 072003, 2011.

[14] S. Sohn, I. Cho, S. Kwon, H. Lee, and S. J. Kim, "Surface Conduction

in a Microchannel," *Langmuir,* vol. 34, no. 26, pp. 7916-7921, 2018.
[15] I. Cho, G. Sung, and S. J. Kim, "Overlimiting Current Through Ion Concentration Polarization Layer: Hydrodynamic Convection Effects," *Nanoscale,* vol. 6, no. 9, pp. 4620-4626, 2014.
[16] I. Rubinstein and B. Zaltzman, "Equilibrium Electroconvective Instability," *Physical Review Letters,* vol. 114, no. 11, p. 114502, 03/16/ 2015.
[17] J. Choi, A. Mani, H. Lee, and J. S. Kim, "Investigation on the Stability of Random Vortices in an Ion Concentration Polarization Layer with Imposed Normal Fluid Flow," *Micromachines,* vol. 11, no. 5, 2020.
[18] R. Kwak, V. S. Pham, K. M. Lim, and J. Han, "Shear Flow of an Electrically Charged Fluid by Ion Concentration Polarization: Scaling Laws for Electroconvective Vortices," *Physical Review Letters,* vol. 110, no. 11, p. 114501, 03/12/ 2013.
[19] K. Huh, S.-Y. Yang, J. S. Park, J. A. Lee, H. Lee, and S. J. Kim, "Surface conduction and electroosmotic flow around charged dielectric pillar arrays in microchannels," *Lab on a Chip,* 10.1039/C9LC01008D vol. 20, no. 3, pp. 675-686, 2020.
[20] S. A. Hong, Y.-J. Kim, S. J. Kim, and S. Yang, "Electrochemical detection of methylated DNA on a microfluidic chip with nanoelectrokinetic pre-concentration," *Biosensors and Bioelectronics,* vol. 107, pp. 103-110, 2018/06/01/ 2018.
[21] J. Choi *et al.*, "Nanoelectrokinetic Selective Preconcentration Based on Ion Concentration Polarization," *BioChip Journal,* vol. 14, no. 1, pp. 100-109, 2020/03/01 2020.
[22] J. Choi *et al.*, "Selective preconcentration and online collection of charged molecules using ion concentration polarization," *RSC Advances,* 10.1039/C5RA12639H vol. 5, no. 81, pp. 66178-66184, 2015.
[23] H. Jeon, H. Lee, K. H. Kang, and G. Lim, "Ion concentration polarization-based continuous separation device using electrical repulsion in the depletion region," *Scientific Reports,* vol. 3, no. 1, p. 3483, 2013/12/19 2013.
[24] S. Baek *et al.*, "Dynamics of driftless preconcentration using ion concentration polarization leveraged by convection and diffusion," *Lab on a Chip,* 10.1039/C9LC00508K vol. 19, no. 19, pp. 3190-3199, 2019.
[25] B. Kim *et al.*, "Purification of High Salinity Brine by Multi-Stage Ion Concentration Polarization Desalination," (in eng), *Scientific reports,* vol. 6, pp. 31850-31850, 2016.
[26] S. J. Kim, S. H. Ko, K. H. Kang, and J. Han, "Direct seawater desalination by ion concentration polarization," *Nature Nanotechnology,* vol. 5, pp. 297-301, 2010.
[27] D. Deng *et al.*, "Overlimiting Current and Shock Electrodialysis in Porous Media," *Langmuir,* vol. 29, no. 52, pp. 16167-16177, 2013.
[28] G. Yossifon, P. Mushenheim, Y. C. Chang, and H. C. Chang, "Eliminating the limiting-current phenomenon by geometric field focusing into nanopores and nanoslots," (in English), *Physical Review E,* Article vol. 81, no. 4, Apr 2010, Art. no. 046301.

[29] S. J. Kim, L. D. Li, and J. Han, "Amplified Electrokinetic Response by Concentration Polarization near Nanofluidic Channel," *Langmuir,* vol. 25, no. 13, pp. 7759-7765, 2009/07/07 2009.
[30] J. Schiffbauer, S. Park, and G. Yossifon, "Electrical Impedance Spectroscopy of Microchannel-Nanochannel Interface Devices," *Physical Review Letters,* vol. 110, no. 20, May 2013, Art. no. 204504.
[31] R. Kwak and J. Han, "Half-Cell Ion Concentration Polarization on Nafion-Coated Electrode," *The Journal of Physical Chemistry Letters,* vol. 9, no. 11, pp. 2991-2999, 2018/06/07 2018.
[32] L. Rosentsvit, S. Park, and G. Yossifon, "Effect of advection on transient ion concentration-polarization phenomenon," *Physical Review E,* vol. 96, no. 2, p. 023104, 08/21/ 2017.
[33] M. Jia and T. Kim, "Multiphysics Simulation of Ion Concentration Polarization Induced by a Surface-Patterned Nanoporous Membrane in Single Channel Devices," *Analytical Chemistry,* vol. 86, no. 20, pp. 10365-10372, 2014/10/21 2014.
[34] R. Dhopeshwarkar, R. M. Crooks, D. Hlushkou, and U. Tallarek, "Transient Effects on Microchannel Electrokinetic Filtering with an Ion-Permselective Membrane," *Analytical Chemistry,* vol. 80, no. 4, pp. 1039-1048, 2008/02/01 2008.
[35] S.-H. Ko and K.-H. Kang, "Visualization of Ion Transport and pH Change in Ion Concentration Polarization," *Journal of the Korean Society of Visualization,* vol. 8, 12/31 2010.
[36] W. Kim, J. Oh, S. Kwon, K. Kim, and S. J. Kim, "Quantifying the pH shift induced by selective anodic electrochemical reactions in the ion concentration polarization phenomenon," *Lab on a Chip,* 10.1039/C8LC01363B vol. 19, no. 8, pp. 1359-1369, 2019.
[37] J. Kim, H.-Y. Kim, H. Lee, and S. J. Kim, "Pseudo 1-D Micro/Nanofluidic Device for Exact Electrokinetic Responses," *Langmuir,* vol. 32, no. 25, pp. 6478-6485, 2016/06/28 2016.
[38] S. Y. Son, H. Lee, and S. J. Kim, "Paper-based ion concentration polarization device for selective preconcentration of muc1 and lamp-2 genes," *Micro and Nano Systems Letters,* vol. 5, no. 1, p. 8, 2017/01/11 2017.
[39] B. Kim *et al.*, "Tunable Ionic Transport for a Triangular Nanochannel in a Polymeric Nanofluidic System," *ACS Nano,* vol. 7, no. 1, pp. 740-747, 2013/01/22 2013.
[40] N. A. Mishchuk, "Perspectives of the electrodialysis intensification," *Desalination,* vol. 117, no. 1, pp. 283-295, 1998/09/20/ 1998.
[41] N. A. Mishchuk, L. K. Koopal, and F. Gonzalez-Caballero, "Intensification of electrodialysis by applying a non-stationary electric field," *Colloids and Surfaces A: Physicochemical and Engineering Aspects,* vol. 176, no. 2, pp. 195-212, 2001/01/30/ 2001.
[42] P. Sistat, P. Huguet, B. Ruiz, G. Pourcelly, S. A. Mareev, and V. V. Nikonenko, "Effect of pulsed electric field on electrodialysis of a NaCl solution in sub-limiting current regime," *Electrochimica Acta,* vol. 164, pp. 267-280, 2015/05/10/ 2015.
[43] S. Alizadeh, M. Z. Bazant, and A. Mani, "Impact of network

heterogeneity on electrokinetic transport in porous media," *Journal of Colloid and Interface Science,* vol. 553, pp. 451-464, 2019/10/01/ 2019.

[44] J. C. T. Eijkel and A. van den Berg, "Nanofluidics and the chemical potential applied to solvent and solute transport," (in English), *Chemical Society Reviews,* Review vol. 39, no. 3, pp. 957-973, 2010.

[45] A. Piruska, M. Gong, J. V. Sweedler, and P. W. Bohn, "Nanofluidics in chemical analysis," (in English), *Chemical Society Reviews,* Review vol. 39, no. 3, pp. 1060-1072, 2010.

[46] E. Kjeang, N. Djilali, and D. Sinton, "Microfluidic fuel cells: A review," *Journal of Power Sources,* vol. 186, p. 353, 2009.

[47] R. B. Schoch, J. Han, and P. Renaud, "Transport phenomena in nanofluidics," *Reviews of Modern Physics,* vol. 80, pp. 839-883, 2008.

[48] T. A. Zangle, A. Mani, and J. G. Santiago, "Theory and experiments of concentration polarization and ion focusing at microchannel and nanochannel interfaces," *Chemical Society Reviews,* vol. 39, pp. 1014-1035, 2010.

[49] !!! INVALID CITATION !!! [40-42].

[50] I. Cho, W. Kim, J. Kim, H.-Y. Kim, H. Lee, and S. J. Kim, "Non-Negligible Diffusio-Osmosis Inside an Ion Concentration Polarization Layer," *Physical Review Letters,* vol. 116, no. 25, p. 254501, 06/20/ 2016.

[51] S. M. Davidson, M. B. Andersen, and A. Mani, "Chaotic Induced-Charge Electro-Osmosis," *Physical Review Letters,* vol. 112, p. 128302, 2014.

[52] S. Alizadeh and A. Mani, "Multiscale Model for Electrokinetic Transport in Networks of Pores, Part I: Model Derivation," *Langmuir,* vol. 33, no. 25, pp. 6205-6219, 2017/06/27 2017.

[53] S. Alizadeh, M. Z. Bazant, and A. Mani, "Impact of Network Heterogeneity on Electrokinetic Transport in Porous Media," *Journal of colloid and interface science,* 2019.

[54] M. B. Andersen, K. M. Wang, J. Schiffbauer, and A. Mani, "Confinement effects on electroconvective instability," *Electrophoresis,* vol. 38, no. 5, pp. 702-711, 2017.

[55] K. Kim, W. Kim, H. Lee, and S. J. Kim, "Stabilization of ion concentration polarization layer using micro fin structure for high-throughput applications," *Nanoscale,* 10.1039/C6NR08978J vol. 9, no. 10, pp. 3466-3475, 2017.

[56] Q. Pu, J. Yun, H. Temkin, and S. Liu, "Ion-Enrichment and Ion-Depletion Effect of Nanochannel Structures," *Nano Letters,* vol. 4, pp. 1099-1103, 2004.

[57] S. Y. Son, S. Lee, H. Lee, and S. J. Kim, "Engineered nanofluidic preconcentration devices by ion concentration polarization," *BioChip Journal,* journal article vol. 10, no. 4, pp. 251-261, 2016.

[58] J. Heo, H. J. Kwon, H. Jeon, B. Kim, S. J. Kim, and G. Lim, "Ultra-high-aspect-orthogonal and tunable three dimensional polymeric nanochannel stack array for BioMEMS applications," *Nanoscale,* 10.1039/C4NR00350K vol. 6, no. 16, pp. 9681-9688, 2014.

[59] A. A. Moya, E. Belashova, and P. Sistat, "Numerical simulation of linear sweep and large amplitude ac voltammetries of ion-exchange membrane systems," *Journal of Membrane Science,* vol. 474, pp. 215-223, 2015.
[60] R. Kant, "Theory for anomalous response in cyclic staircase voltammetry: electrode roughness and unequal diffusivities," *The Journal of Physical Chemistry C,* vol. 118, no. 46, pp. 26599-26612, 2014.
[61] S. Mikhaylin *et al.*, "How physico-chemical and surface properties of cation-exchange membrane affect membrane scaling and electroconvective vortices: Influence on performance of electrodialysis with pulsed electric field," *Desalination,* vol. 393, pp. 102-114, 2016/09/01/ 2016.
[62] V. V. Nikonenko *et al.*, "Desalination at overlimiting currents: State-of-the-art and perspectives," *Desalination,* vol. 342, pp. 85-106, 2014/06/02/ 2014.
[63] N. A. Mishchuk, S. V. Verbich, and F. Gonzales-Caballero, "Concentration Polarization and Specific Selectivity of Membranes in Pulse Mode," *Colloid Journal,* vol. 63, no. 5, pp. 586-595, 2001/09/01 2001.
[64] P. A. Sosa-Fernandez, J. W. Post, M. S. Ramdlan, F. A. M. Leermakers, H. Bruning, and H. Rijnaarts, "Improving the performance of polymer-flooding produced water electrodialysis through the application of pulsed electric field," *Desalination,* vol. 484, p. 114424, 06/01 2020.
[65] H.-J. Lee and S.-H. Moon, "Enhancement of electrodialysis performances using pulsing electric fields during extended period operation," *Journal of Colloid and Interface Science,* vol. 287, no. 2, pp. 597-603, 2005/07/15/ 2005.
[66] S. Mikhaylin, V. Nikonenko, G. Pourcelly, and L. Bazinet, "Intensification of demineralization process and decrease in scaling by application of pulsed electric field with short pulse/pause conditions," *Journal of Membrane Science,* vol. 468, pp. 389-399, 10/01 2014.
[67] A. M. Uzdenova, A. V. Kovalenko, M. K. Urtenov, and V. V. Nikonenko, "Effect of electroconvection during pulsed electric field electrodialysis. Numerical experiments," *Electrochemistry Communications,* vol. 51, pp. 1-5, 2015/02/01/ 2015.
[68] S. V. Zyryanova, D. Y. Butyl'skii, S. A. Mareev, N. D. Pis'menskaya, V. V. Nikonenko, and G. Pourcelly, "Effect of Parameters of Pulsed Electric Field on Average Current Density through Nafion 438 Membrane in Electrodialysis Cell," *Russian Journal of Electrochemistry,* vol. 54, no. 10, pp. 775-781, 2018/10/01 2018.
[69] P. Malek, J. M. Ortiz, B. Richards, and A. Schaefer, "Electrodialytic removal of NaCl from water: Impacts of using pulsed electric potential on ion transport and water dissociation phenomena," *Journal of Membrane Science,* vol. 435, pp. 99-109, 05/01 2013.
[70] C. L. Druzgalski, M. B. Andersen, and A. Mani, "Direct numerical simulation of electroconvective instability and hydrodynamic chaos near an ion-selective surface," vol. 25, no. 11, p. 110804, 2013.

[71] E. Yariv, "Asymptotic current-voltage relations for currents exceeding the diffusion limit," *Physical Review E,* vol. 80, no. 5, p. 051201, 11/06/ 2009.
[72] D. A. Riehm and A. V. McCormick, "The role of dispersants' dynamic interfacial tension in effective crude oil spill dispersion," *Marine Pollution Bulletin,* vol. 84, no. 1, pp. 155-163, 2014/07/15/ 2014.
[73] M. Roulia, K. Chassapis, C. Fotinopoulos, T. Savvidis, and D. Katakis, "Dispersion and Sorption of Oil Spills by Emulsifier-Modified Expanded Perlite," *Spill Science & Technology Bulletin,* vol. 8, no. 5, pp. 425-431, 2003/01/01/ 2003.
[74] R. M. Atlas, "Microbial hydrocarbon degradation—bioremediation of oil spills," vol. 52, no. 2, pp. 149-156, 1991.
[75] R. S. Hyam, K. M. Subhedar, and S. H. Pawar, "Effect of particle size distribution and zeta potential on the electrophoretic deposition of boron films," *Colloids and Surfaces A: Physicochemical and Engineering Aspects,* vol. 315, no. 1, pp. 61-65, 2008/02/15/ 2008.
[76] N. Rocha, R. Ribeiro, N. Merlo, and M. Franco, "Oil Removing from Emulsions Using Commercial Resins," *Journal of Chemistry and Chemical Engineering,* vol. 10, 04/28 2016.
[77] K.-Y. A. Lin, H. Yang, C. Petit, and F.-K. Hsu, "Removing oil droplets from water using a copper-based metal organic frameworks," *Chemical Engineering Journal,* vol. 249, pp. 293-301, 2014/08/01/ 2014.
[78] R. M. Bande, B. Prasad, I. M. Mishra, and K. L. Wasewar, "Oil field effluent water treatment for safe disposal by electroflotation," *Chemical Engineering Journal,* vol. 137, no. 3, pp. 503-509, 2008/04/15/ 2008.
[79] H. Peng *et al.*, "Preparation of Superhydrophobic Magnetic Cellulose Sponge for Removing Oil from Water," *Industrial & Engineering Chemistry Research,* vol. 55, no. 3, pp. 832-838, 2016/01/27 2016.
[80] P. Janknecht, A. D. Lopes, and A. M. Mendes, "Removal of Industrial Cutting Oil from Oil Emulsions by Polymeric Ultra- and Microfiltration Membranes," *Environmental Science & Technology,* vol. 38, no. 18, pp. 4878-4883, 2004/09/01 2004.
[81] Q. Ma, H. Cheng, A. G. Fane, R. Wang, and H. Zhang, "Recent Development of Advanced Materials with Special Wettability for Selective Oil/Water Separation," vol. 12, no. 16, pp. 2186-2202, 2016.
[82] M. Dudek and G. Øye, "Microfluidic Study on the Attachment of Crude Oil Droplets to Gas Bubbles," *Energy & Fuels,* vol. 32, no. 10, pp. 10513-10521, 2018/10/18 2018.
[83] G. Goet, T. Baier, S. Hardt, and A. K. Sen, "Isotachophoresis with emulsions," *Biomicrofluidics,* vol. 7, no. 4, p. 044103, 2013/07/01 2013.
[84] D. Di Carlo, D. Irimia, R. G. Tompkins, and M. Toner, "Continuous inertial focusing, ordering, and separation of particles in microchannels," vol. 104, no. 48, pp. 18892-18897, 2007.
[85] S. S. Dukhin, "Electrokinetic phenomena of the second kind and their applications," *Advances in Colloid and Interface Science,* vol. 35, pp.

173-196, 1991/03/01/ 1991.
[86] K. Kamogawa *et al.*, "Surfactant-free O/W emulsion formation of oleic acid and its esters with ultrasonic dispersion," *Colloids and Surfaces A: Physicochemical and Engineering Aspects,* vol. 180, no. 1, pp. 41-53, 2001/05/15/ 2001.
[87] J. I. Acedo-Carrillo, A. Rosas-Durazo, R. Herrera-Urbina, M. Rinaudo, F. Goycoolea, and M. Valdez, "Zeta potential and drop growth of oil in water emulsions stabilized with mesquite gum," *Carbohydrate Polymers,* vol. 65, pp. 327-336, 08/01 2006.
[88] A. Wiącek and E. Chibowski, "Zeta potential, effective diameter and multimodal size distribution in oil/water emulsion," *Colloids and Surfaces A: Physicochemical and Engineering Aspects,* vol. 159, no. 2, pp. 253-261, 1999/12/01/ 1999.
[89] F. Sousa, S. Moreira, S. Dos, S. Da, J. Nero, and P. Alcantara Jr, "Dielectric Properties of Oleic Acid in Liquid Phase," *Journal of Bionanoscience,* vol. 3, 12/01 2009.
[90] G. Hahn, P. Svejda, and A. Dallos, "Volumetric and dielectric properties of the binary liquid systems: 1,2-dichloroethane + n-alkanes or + 2,2,4-trimethylpentane," *Fluid Phase Equilibria,* vol. 86, pp. 293-313, 1993/07/01/ 1993.
[91] C. Wohlfarth, "Dielectric constant of 2,2,4-trimethylpentane," *Landolt Börnstein,* 01/01 2008.
[92] J. M. Kokosa, A. J. Przyjazny, and M. A. Jeannot, *Solvent microextraction : theory and practice*. Hoboken, N.J.: Wiley, 2009.
[93] H. Lizhi, K. Toyoda, and I. Ihara, "Dielectric properties of edible oils and fatty acids as a function of frequency, temperature, moisture and composition," *Journal of Food Engineering,* vol. 88, no. 2, pp. 151-158, 2008/09/01/ 2008.

초록

이온 선택성 막 주변에서 발생하는 나노전기동력학적 현상의 일시적 반응 연구

성 명 권순현
학과 및 전공 전기·컴퓨터공학부
공과대학원
서울대학교

나노 다공성 투과막은 벽면 전하의 영향을 받아 막의 구멍 내부에서 전위를 띄게 되고, 이에 따라 벽면 전하와 반대되는 전하를 띤 이온들만 막의 통과가 가능하게 된다. 이런 막의 전기적인 현상으로 인해 전기를 인가하였을 때, 선택적 이온 통과 현상이 발생하게 된다. 그 중 이온 농도 분극 현상은 최근 수십 년간 활발히 연구된 현상으로, 유동과 이온의 이동 그리고 전위가 복합적으로 작용하여 만들어진다. 이에 따라 기초 연구부터 응용장치까지, 예를 들면 탈염기, 분리기, 농축기, 바이오센서 등이 발달해왔다. 이런 응용장치들은 많은 연구가 진행되어 왔고, 향상되어왔다.

이런 장치들은 일반적으로 정상 상태보다 일시적 상태에서 발생되게 되는데, 일시적 상태에서는 정상상태와는 다른 새로운 물리적 현상들이 발생하게 된다. 일시적 상황에서는 정상 상태에서 예상치 못한 현상들이 발견되고, 이에 따라 장치의 작동이 방해를 받아 효율이 떨어지는 현

상이 발생한다. 따라서 이온 농도 분극 현상 응용장치들의 효율 최적화를 위해서는, 일시적 상태의 이동 현상과 전류 특성에 대한 연구가 불가피하다. 이 논문에서는 이온 농도 분극 현상에서 이온의 움직임을 간접적으로 살펴보는 전류 특성에 대한 연구로, 일시적 상태일 때 나타나는 전류의 특징을 실험적으로 살펴보고, 나아가 경계조건을 연속적으로 바꾸어 주어 전류의 변화를 수치적, 실험적으로 살펴보았다.

첫 번째로 일시적 현상에서 발생하는 오버슛(overshoot) 전류에 대해 살펴보았다. 전류-전압 곡선은 정상상태에서 옴(Ohm) 구간, 한계전류구간, 과도한계전류 구간으로 나타나는데, 실험적으로 전류-전압 특성을 살펴보게 되면 예상치 못한 치솟는 전류, 오버슛 전류가 옴과 한계전류 구간 사이에서 발생하게 된다. 이온 농도 분극 현상을 이용한 응용장치의 최적 효율은 보통 한계 전류나 과도한계전류 구간에서 발생하는데, 상황에 따라 최적 효율이 나타나는 구간이 다르다. 이에 전류-전압 특성을 정확하게 측정 후 작동하는 전압을 선택하는 것이 중요한데 이 오버슛 전류는 이를 방해한다. 농도 분극 장치에서 오버슛 전류에 가장 큰 영향을 미치는 변수를 찾고, 이를 없애기 위한 장치를 개발하기 위해 연구를 진행하였다. 이 연구에서는 유동을 이용하여 이온 농도 분극 현상으로 인해 농도가 바뀌는 구간(유효 채널)을 제한하였다. 전압 상승 속도를 일정하게 한 후 장치의 모양을 조금씩 바꾸어 줌으로써, 유효 채널 길이를 바꾸었고, 전류-전압특성을 살펴본 결과 최적의 길이를 찾았다. 이를 통해 오버슛 전류가 확산층의 확산 완화 시간과 관계가 있음을 확인하였고, 채널 길이를 조절하면 정상상태에 도달하기 위해 필요한 확

산 완화 시간이 줄어 오버슛을 없앨 수 있음을 확인하였다. 또한 길이를 일정하게 하고 전압 상승 속도도 바꾸어 가면 실험하여, 앞의 결과를 다시 한번 확인하였다. 이 연구를 통해 개발된 장치로 정상 상태에 빠르게 도달하여, 정상상태 전류-전압 특성을 살펴보는 기초 연구에 필요한 시간을 기존 미세유체장치 연구들에 비해 20배 이상 단축시킬 수 있었고, 이온 농도 분극 장치를 만들 때, 확산 층의 길이를 최대한 고려해서 제작하면 오버슛이 없는 전류-전압 곡선을 얻을 수 있는 전압상승 속도를 계산할 수 있음을 확인할 수 있었다.

두 번째 연구는 과도한계전류 구간 중 전기 와류 영역에 관한 연구이다. 이온 농도 분극 현상이 발생하면, 이와 함께 전기 와류라고 하는 불안정한 유동이 발생한다. 이 불안정한 유동은 이온전달현상을 향상 시키는데, 이때 인가하는 전압을 펄스 형태를 취하게 되면 막 주변에서 물 분해가 적게 발생하고, 막이 불순물로 막히는 현상, 막을 통과하는 전류가 증가하는 현상 등 탈염기에 있어 효율이 증가하는 현상들이 발생한다. 그 중 전류가 증가하는 원인에 대해서는 불명확하고 활발한 토론이 진행중에 있다. 막을 통과하는 전류는 곧 탈염의 효율과 직접적인 연관이 있기에, 이 연구에서는 전기와류에 대한 펄스 전압을 인과하였을 때 나타나는 전류 밀도 증가 현상을 실험과 전산모사를 통해 살펴보았다. 전산모사와 실험을 통해 전압의 진동수와 전류 간에 특정한 경향성을 가지는 것을 확인할 수 있었다. 이에 대하여 전산 모사를 통해 농도의 변화 및 와류의 속도 변화를 살펴보았고, 실험적으로 이를 가시화하였다. 진동수를 바꿔 감에 따라 최적 값이 나타나는 것을 확인하였고, 이는 전기 와

류의 성장과 유지와 관련이 있다는 것을 확인하였다. 전기 와류 장치의 구조에 따라 적절한 진동수를 선택한다면 좀 더 높은 효율의 전류 밀도를 측정할 수 있고, 이온 이동을 꾀할 수 있다.

이와 같은 연구들을 통해 복잡한 물리적 현상 중 하나인 이온 농도 농도 분극 현상의 일시적 상태에 대해 연구를 진행하였다. 일시적 상황에서 막을 통한 이온의 이동의 변화에 대해 확인하였고, 이를 통해 탈염기나 분리기 등 응용장치의 효율 향상에 도움이 될 것이라고 예상된다.

Keywords : 전기동역학, 이온농도분극현상, 오버슛 전류, 전기와류, 일시적 현상.
Student Number : 2013-23098